Russian Chemical Reviews **63** (9) 711 – 734 (1994)
©1994 Russian Academy of Sciences and Turpion Ltd

UDC 541.16

The chemical bonding and electronic properties of metal borides

G P Shveikin, A L Ivanovskii

Contents

I.	Introduction	711
II.	Group I and II metal and aluminium borides	712
III.	Transition *d* metal borides	716
IV.	Metal–nonmetal–boron ternary systems	724
V.	Metal–metal–boron ternary systems	727
VI.	Amorphous metal borides	728

Abstract. The results of theoretical and experimental studies on the electronic structure, and nature of interatomic interactions, and the properties of binary metal borides, ternary boron-containing compounds and alloys, and also amorphous binary and multicomponent borides are examined. The prospects for employing the methods of solid-state quantum-chemistry in the description of the fundamental electronic properties of metal borides are discussed. The bibliography includes 255 references.

I. Introduction

Metal borides belong to one of the most interesting classes of solid compounds and possess a set of important physicochemical properties (thermomechanical, magnetic, electrophysical, and others), which permits their wide scale employment as components of refractory alloys, in the development of special purpose ceramics and metalloceramics, as protective coatings for high-temperature alloys, as a base for composite materials, as solid solders, and as corrosion-resistant and abrasive materials.[1–14]

In terms of their thermal properties, strength, plastic properties, and electrical and thermal insulating characteristics, borides compete with other classes of high-temperature compounds—carbides and nitrides.[15,16] The borides possess a series of specific properties determined, in particular, by the nature of the chemical bonding and the electronic structure.

Boron is known to form predominantly covalent compounds with metals, an important role being assumed in this process not only by M–B and M–M bonds (M = metal) but also by direct B–B interactions. The latter are evidently responsible for the great diversity of the structural types of borides,[5,7,9,11,12] in which boron atoms can be both surrounded by metallic centres and can form linear, planar, or three-dimensional structures (Fig. 1).

The ability of many metals to form, in their interaction with boron, a large set of phases with a considerable variation of the M/B ratio—ranging from hemiborides (M_2B) to dodecaborides (MB_{12})—as well as amorphous alloys, is well known.[1–14]

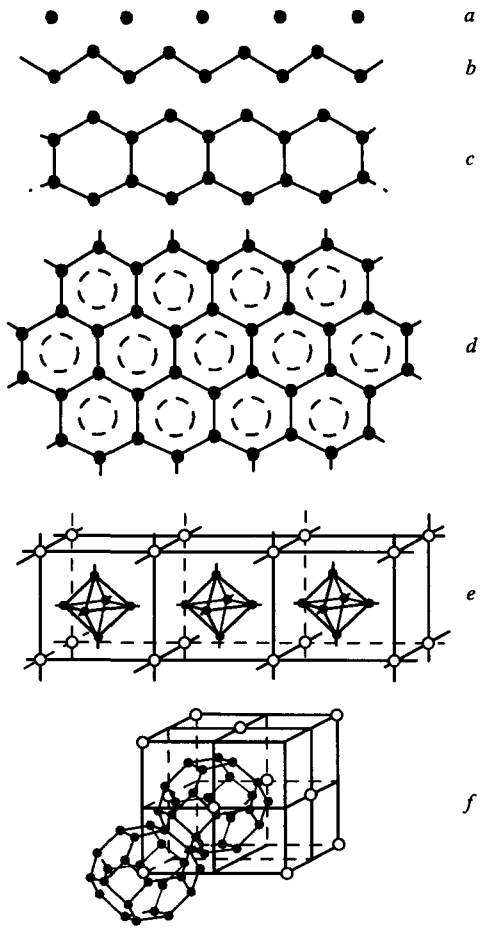


Figure 1. The possible configurations of boron atoms in the structures of the metal borides M_2B (*a*), MB (*b*), M_3B_4 (*c*), MB_2 (*d*), MB_4–MB_6 (*e*), and MB_{12} (*f*).

Relations of the composition–property type are therefore of extreme interest for metal–boron systems.

In the early stages of the relevant investigations, several alternative phenomenological models were proposed for the description of the nature of the interatomic bonds and charge states in borides. Thus the formation of borides containing planar

G P Shveikin, A L Ivanovskii Institute of Solid State Chemistry, The Urals Division of the Russian Academy of Sciences, Pervomaiskaya 91, 620219 Ekaterinburg, Russian Federation, Fax (7-343) 244 44 95

Received 27 June 1994
Uspekhi Khimii **63** (9) 751 – 775 (1994); translated by A K Grzybowski

networks made up of boron atoms has been attributed [17,18] to the formation of sp^2 configurations of the boron atoms, while the appearance in the higher borides of three-dimensional groups of boron atoms (octahedra, cubooctahedra, etc.) has been attributed to the formation of the electronic sp^3 configuration. The existence of graphite-like motifs of boron atoms in a type AlB_2 lattice has been explained [19] by the presence of metal atoms as electron donor and of boron atoms as electron acceptors. Conversely, in the 'interstitial alloy' model,[20] the transfer of additional electron density to metal atoms is postulated.

The correlation of the properties with the specific features of the chemical bonding in borides has been interpreted from the standpoint of the dominant character of the B–B bonds in the overall system of interactions in the crystals,[19,21] whereas in other studies [22,23] preference has been given to covalent metal–boron bonds. Dempsey [20] believed that M–M bonds play a decisive role in bonding (especially for the lower borides). It is noteworthy that, although each of the models examined has had some success in the treatment of the characteristic features of the variation of a specific set of properties of individual groups of borides, they are nevertheless far from being universal.

The aim of the present review is to attempt a consideration of the current state of the theory of the electronic structure, the chemical bonding, and the most important physicochemical properties of the main groups of *s*, *p*, and *d* metal borides on the basis of the study of their fundamental electronic properties within the framework of computational solid state quantum-chemical methods and the most correct experimental methods for the investigation of the electronic structure of crystals—X-ray emission, electronic, and optical spectroscopy and a series of other methods.

The borides have been segregated into individual groups in conformity with the classification adopted and are considered in the following sections:[14,24,25] Group I and II binary metal borides in Section II, *d* metal borides in Section III, ternary metal–non-metal boron systems in Section IV, metal–metal–boron systems in Section V, and amorphous metal borides (metallic glasses) in Section VI.

II. Group I and II metal and aluminium borides

1. Sodium and potassium borides

The study of the phase diagrams for the alkali metal–boron systems indicates [1–11] the greatest probability of the formation and stability of the borides MB_6. The band structure of the hypothetical sodium hexaboride (CsCl type lattice with interatomic distances corresponding to those found for CaB_6) [7] has been calculated [26] by the tight binding method. The valence band contains 10 partly occupied subbands, the dispersion of which is significantly smaller than in the isostructural calcium hexaboride (see below), the highest occupied states including also the 2*s* states of boron. The 3*s* states of sodium are located predominantly in the conduction band.

There is no forbidden gap in NaB_6. The concentration of valence electrons per unit cell is 19 e, so that some of the highest bonding bands (forming a planar section in the vicinity of the Fermi level) remain unoccupied, which may be the reason for the instability of the phase. The lowest virtual NaB_6 bands are separated from the system of valence states, which makes it likely that the type of conductivity of NaB_6 is intermediate between that of semicon-ductor systems based on Group II metals and that of the quasi-metallic lanthanum hexaborides.

The electronic spectrum of KB_6 has been calculated [26] by the tight binding method. A considerable similarity between the topologies of the NaB_6 and KB_6 bands has been noted. The introduction of the *d* states of potassium into the basis set in the calculation diminishes the width of the forbidden gap at the point *X*. The Fermi level (−8.1 eV) is located near the lower edge of the forbidden gap in the region of a high concentration of electronic states. It is postulated that the stability of the KB_6 lattice is caused primarily by the transfer of some of the 'metallic' electrons (the effective charges on the component atoms are +0.74 e for K and −0.74 e for B) to the bonding states between the boron atoms in the B_6 octahedra and the bonds between the given groups, which are manifested by two intense maxima in the distribution of the density of 2*p* states of boron (Fig. 2). We may note that this treatment conflicts with the Longuet-Higgins and Roberts model,[27] which postulates the existence of the doubly charged anions B^{2-} in the structure of stable hexaborides. The insignificant concentration of holes in the valence band may indicate that the boride is a semiconductor.

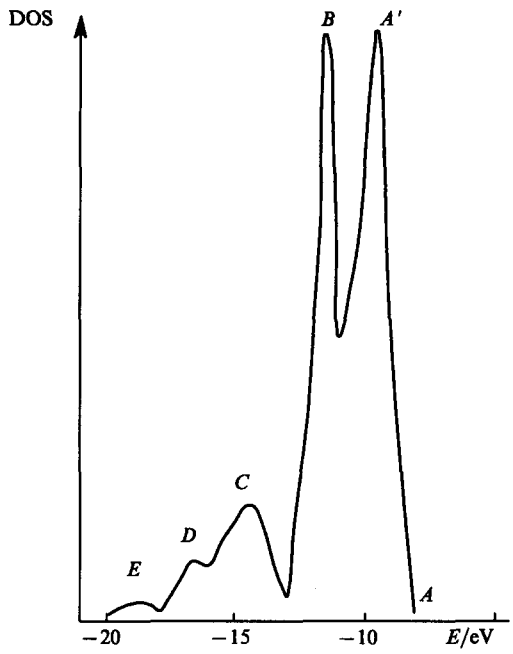


Figure 2. Distribution of the density of B 2*p* states for KB_6.[26]

2. Beryllium borides

According to the literature,[2,7,10] there are at least six individual compounds in the Be–B system (ranging from Be_5B to BeB_9), which differ sharply in their crystal structures and physicochemical properties. However, the increase with increasing boron content of the melting point and of the enthalpy of atomisation of the phase, as well as the change in the type of conductivity (from metallic to semiconducting), etc. still cannot be explained from the standpoint of electronic properties.

The treatment of the electronic processes accompanying the diffusion of boron and beryllium was initially based on the ideas of the configuration theory,[1,17] in which the primary single-electron transition $s \rightarrow p$ with formation of the Be $2s^12p^1$ configuration and subsequent 'trapping' of the boron electrons with the formation of stable sp^2 or sp^3 configurations is postulated.

In the single calculation [28] known to us, the cubic Be_2B phase (structure of the *anti*-CaF_2 type) was considered. Calculations were performed by the self-consistent method of the linearised muffin-tin orbitals (LMTO) and the chemical bonding was analysed within the framework of the self-consistent field X_α-discrete variation (SCF X_α-DV) method.

The calculated data [28] show that the valence band of the boride contains two segregated subbands separated by a minimum in the density of states (DOS) and comprising mainly the *s* and *p* states of the components. The Fermi level is located in the region of the (B, Be) 2*p*-like band. Both the *s* and *p* states of the component atoms overlap significantly, which indicates the formation of covalent bonds of the mixed *s*–*s*, *s*–*p*, and *p*–*p* types.

Comparative analysis of the involvement of individual atomic orbitals in such covalent mixing permits the calculation of the Mulliken bond populations.[28] It follows from these that the greatest contribution to the B–B and Be–Be bonding in Be_2B comes from the overlap of the $2p$ functions; the overlap populations of the $s-s$ orbitals are also of comparable magnitude. The involve-ment of all (s, p) valence states is observed in the Be–B interaction, the outer $2p$ orbitals overlapping to the greatest extent under these conditions.

It is seen from the calculations of the electronic configurations and the effective atomic charges of the $[BBe_4B_6]$ cluster that the unoccupied (in the atomic states) $2p$ orbitals of beryllium are appreciably populated (~ 1 e) with formation of configurations close to Be $2s^12p^1$. Estimation of the effective atomic charges indicates the partial transfer of charge density to the boron atoms, which indicates the presence of an ionic bond component.

Thus the calculations[28] make it possible to claim that a covalent-ionic type of chemical bonding is characteristic of Be_2B. The covalent component arises due to the overlap of the outer $2s$ and $2p$ functions of the component atoms involved in the Be–Be, Be–B, and B–B interactions. The contribution of the ionic component is due to the polarisation of electron density in the crystals with partial charge transfer in the direction Be → B.

The ideas about the principal effects of orbital hybridisation yield contour maps of the wave functions of the cluster $[BBe_4B_6]$ for which the calculation has been made (Fig. 3). Evidently the lowest valence molecular orbitals $7a_1$ and $3b_2$ are non-bonding and are largely made up of the B $2s$ states with addition of Be $2s$ orbitals. The contours of the molecular orbitals with $9a_1$ symmetry embrace Be–Be pairs of atoms, illustrating the formation of directed covalent σ^{Be-Be}-bonds, in which the $2s$ and $2p$ states of beryllium participate, while the boron states hardly contribute to this molecular orbital. The wave functions of the $2a_1$ molecular orbital (consisting to the extent of 85% of Be s states) have a typical nonbonding character: the contours of the atomic orbitals of the individual centres are separated by lines with a zero value of the wave function. The Be $2s$, Be $2p$, and B $2p$ atomic orbitals contribute to the $11a_1$ molecular orbital, the configuration of the wave function contours indicating the occurrence in the given energy range of combined (Be–B, B–B) interactions. Finally the wave function contours of the highest occupied $12a_1$ molecular orbital (of the B $2p$ type) are distorted in the direction of the 'outer' (in the cluster) boron atoms, which can be treated as indicating the presence of B–B bonds.

Summarising the foregoing, one may claim that 'covalent interactions occur in Be_2B both between the individual components (Be–Be, B–B) and in the Be–B bond.

There is no doubt that further systematic studies are essential in order to gain a complete idea about the electronic properties of beryllium borides.

3. Calcium, strontium, and barium borides

Calcium, strontium, and barium borides have the composition MB_6 (cubic lattice of the NaCl type). It was in fact because of the simplicity of their crystal structure that calcium hexaboride became one of the first boron-containing compounds the energy structure of which was considered within the framework of theoretical approaches.[27,29–31]

The calculation for CaB_6 was performed by the linear combination of atomic orbitals (LCAO) method with a basis set incorporating the $2s$ and $2p$ orbitals of boron without taking into account the Ca–B interactions.[27] Thus in essence only the structure of the bands formed by the states of the boron sublattice was examined,[27] while the presence of the metal was taken into account in the filling of the energy levels in terms of the rigid band approximation.

Solutions of the secular equation for the crystal made it possible to devise a qualitative scheme for the structure of the energy bands of CaB_6,[27] which showed that a forbidden gap (~ 4.4 eV) appears between the bonding and antibonding orbitals. Since CaB_6 is a conducting substance,[1–4] the authors[27] explained these contradictions both by the possibility of the population of the lowest unoccupied states by the metal electrons and by the probable transfer of valence electrons to the conduction band on irradiation of the crystal.

In describing the energy bands of CaB_6, Yamazaki[29] took into account the Ca $4s$ states in addition to the B s and B p states. It was shown that the bonding bands of the hexaboride are fully occupied while the antibonding ones are unoccupied. This explains the stability of this structural type of borides (in conformity with phenomenological ideas,[32] the hexaborides can be regarded as the complexes $M^{2+}B_6^{2-}$ containing doubly charged metal cations). According to Yamazaki,[29] the width of the forbidden gap is ~ 1.5 eV.

In Flodmark's calculations,[30,31] the CaB_6 band structure was considered as a function of the choice of the exponent $z/3$ for the d orbitals ($z = 1-5$). It was noted that the inclusion of the M shells in the basis set has a very appreciable effect on the energies of the valence bands, leading, in particular, to a further decrease in the width of the forbidden gap.

The conclusions reached[27,29] about the structure of the CaB_6 valence band are consistent with the results of the calculation performed by the LCAO method taking into account only the boron functions[33] and also by the semiempirical

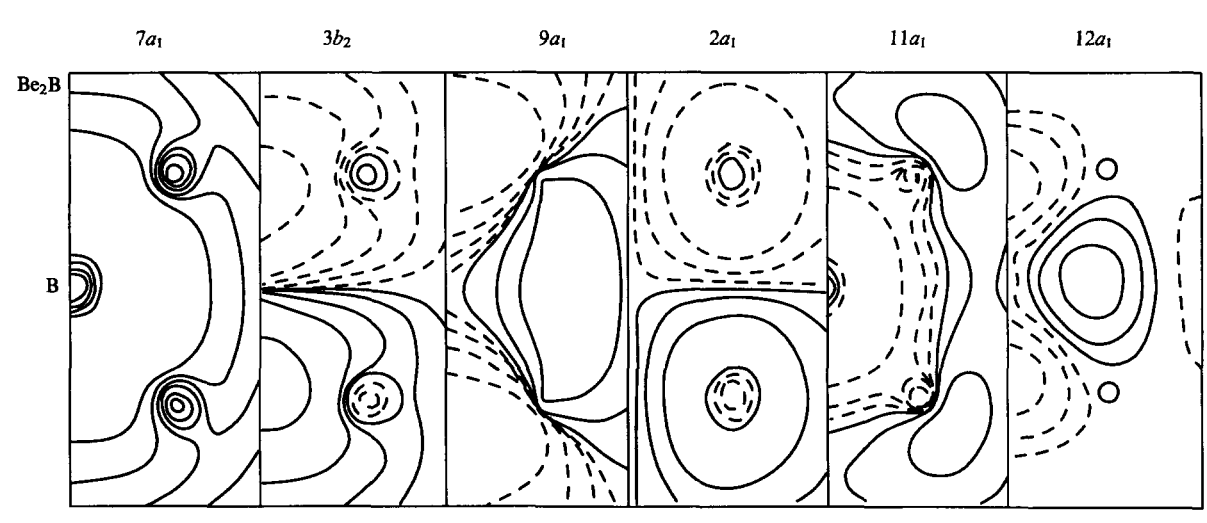


Figure 3. Contour maps for the wave functions of the valence orbitals of the BBe_4B_6 cluster according to the X_α-DV calculation.[28]

LCAO method in terms of the Gaussian orbitals basis set (GO-LCAO),[34] using a basis set comprising the *sp* functions of boron and calcium.

The LCAO method in terms of the tight binding approximation has been used[35] in calculations for CaB_6, where account was taken of the B 2*s*, B 2*p*, and Ca 3*s* states. At the same time, in order to discover the role of calcium in the organisation of the electronic centre of the hexaboride, a band calculation was performed[35] for a hypothetical 'boride' with the parameters of the CaB_6 lattice in which the metal sublattice sites remained unoccupied.

As the energy bands of this 'boride' are filled on the hypothesis that the number of valence electrons of the system (per formula unit) corresponds to that for MB_6 (20 e), it is found that the lowest ten bands are fully occupied. In this case, the minimum 'straight' forbidden gap corresponds to the splitting of the states at the point *X* and its width is 2.11 eV, which exceeds somewhat the values obtained by Johnson and Daane.[36] This discrepancy may be eliminated by including the highest states of the metal (*p* and *d*) in the basis set.[35]

Comparison of the 'B_6' and CaB_6 bands indicates an appreciable role of the metallic states in bonding, which is manifested by an increase in dispersion for a series of bands (along the Λ, Σ, and Δ directions) and also by the initiation of the appearance of new levels in the conduction band.

Calculations have shown[35] that the Ca → B_6 charge transfer does not exceed 0.9–1.0 e, although according to Longuet-Higgins and Roberts[27] the transfer of two electrons is required to stabilise the CaB_6 structure—for the complete filling of the bonding states band. This electron deficiency leads mainly to a weakening of the $p_\sigma p_\sigma$ and $p_\pi p_\pi$ bonds between the B_6 groups without having a significant influence on the 'intracluster' interaction, i.e. without leading to a critical destabilisation of the structure as a whole. This situation is analogous to that for alkali metal hexaborides, where the M → B_6 charge transfer does not exceed 1 e.[35]

The CaB_6 band structure, calculated by the augmented plane wave (APW) method with a Slater exchange-correlation contribution (α = 2/3),[37] differs significantly from that presented in other communications.[27,29–31,35] The absence of a forbidden gap between the valence and conduction bands and also the appreciable concentration of pre-Fermi states (at the point Γ), which conflicts with X-ray electron spectroscopic data, are noteworthy. These discrepancies have been explained[37] by the absence of self-consistency in the calculation for the boride.

A self-consistent study of the influence of metallic *d* states on the electron spectrum of CaB_6 has been carried out by Hasegawa and Yanase,[38] who carried out the calculation by the self-consistent symmetrised APW method. The relativistic effects were described in terms of the scheme presented by Koelling and Harman.[39] The calculations were performed in terms of both the standard muffin tin (MT) approximation and with a correction for the nonsphericity of the potential.

Both calculations yield fairly similar structures of the CaB_6 valence band (Fig. 4), containing a low-energy (lower by ~1.05 Ryd than E_F; Ryd = Rydberg number) B 2*s* band and a system of occupied bands (which are filled by 18 electrons per unit cell) in the range E_F–0.70 Ryd. The lowest virtual band is characterised by an appreciable dispersion due to the effect of the *p*–*d* hybridisation typical for the hexaborides with a very significant contribution by the Ca 3*d* function at the point *X*. The resolution of the states in the MT spheres into individual components also indicates the involvement of the Ca 3*d* orbitals in the pre-Fermi level X_3.

The most remarkable difference in the results of the calculation taking into account the nonsphericity of the potential is the increase in the energy of the X_3 state with appearance of a forbidden gap [$\Delta E(X_3 - X_{3'}) \approx 0.02$ Ryd (Fig. 4)]. The observed changes in the fine structure of the density of states are caused, in particular, by the increase in the amplitude of the Ca *d* states with decrease in the potential, whereupon the given functions assume the form of plane waves.

According to the MT calculation,[38] the surface of the CaB_6 Fermi level consists of electron and hole layers (Fig. 5). The number of carriers is ~2×10^3 electrons and the same number of holes are present in the unit cell. The role of the spin–orbital interactions in the establishment of the pre-Fermi bands has been analysed.[38] It was noted that, when the spin–orbital interactions are taken into account for a slight (~0.01 Ryd) overlap of the valence and conduction bands (according to

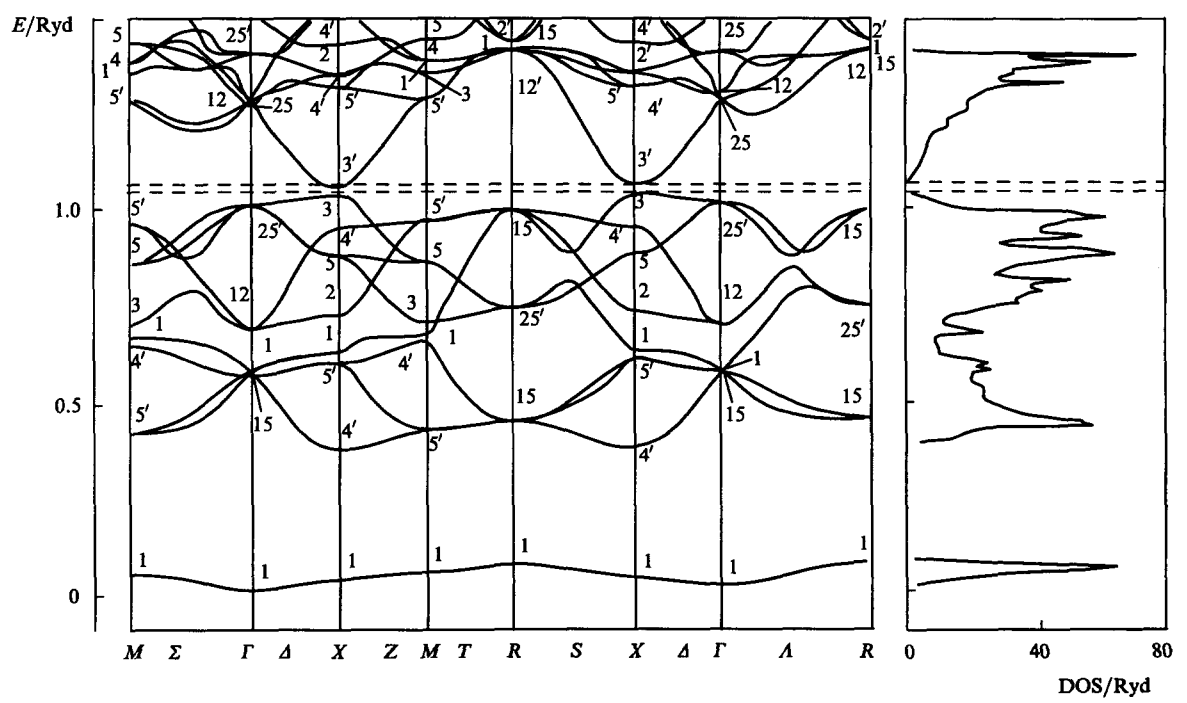


Figure 4. The band structure and the total density of states in CaB_6. SCF-APW calculation with a correction for the nonsphericity of the potential.

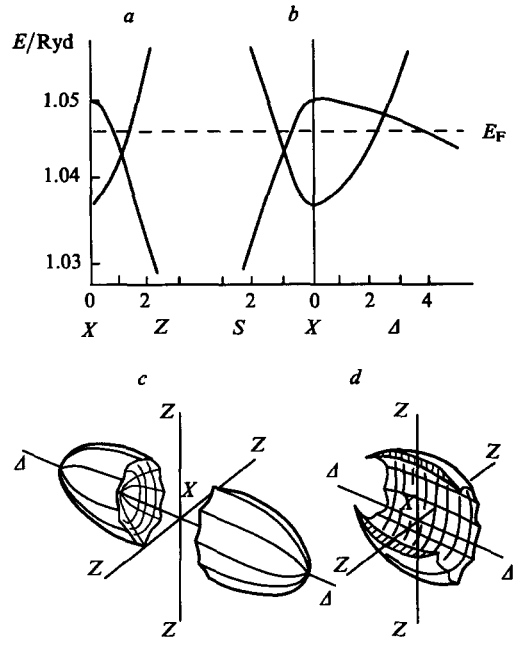


Figure 5. Energy bands near the bottom of the conduction band (*a*) and the upper edge of the valence band (*b*) and schematic representation of the hole (*c*) and electrons (*d*) layers on the Fermi surface in the vicinity of the symmetry point *X* for CaB_2.[38]

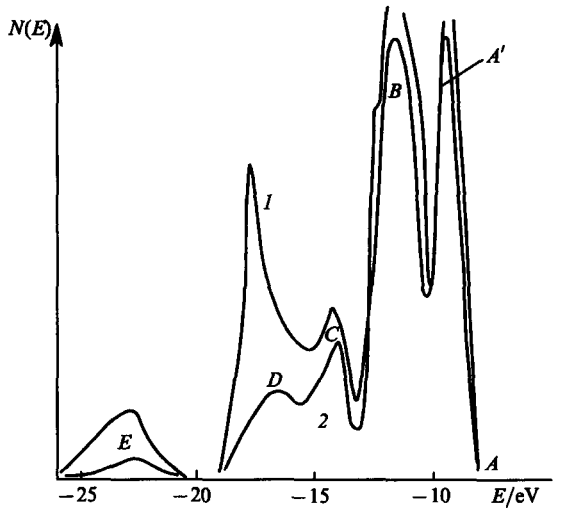


Figure 6. The total (curve *1*) and local (curve *2*) densities of B 2*p* states in BaB_6.[35]

calculations with the MT approximation), a forbidden gap should appear with an indirect transition energy of $\sim 0.001\ R_\infty$, which makes it possible to assign CaB_6 to the class of semiconductors.

The following borides have been investigated by X-ray emission, absorption, and electron spectroscopy: CaB_6,[37,40] BaB_6,[41] ScB_2,[44,46,78] TiB_2,[42–46] VB_2,[46–53] Cr_2B, CrB, CrB_2,[44–46,49,51,54,56,79] Mn_4B, Mn_2B, MnB, Mn_3B_4, MnB_2, MnB_4,[46,54,57,58] Fe_2B, FeB,[43–45,55,58–68] Co_3B, Co_2B, CoB,[44,54,60,65,67,69,70] Ni_3B, Ni_2B, Ni_4B_3, NiB,[44,45,54,58,59,67,71,78,80–82] YB_6,[40] ZrB_2,[37,51,74–76] Nb_2B, Nb_3B_2, Nb_3B_4, NbB, NbB_2,[51,72,73] MoB,[77] HfB_2,[51] and TaB_2.[51,74]

The conducting properties of calcium hexaboride have been treated[1–14] as being either of the semimetallic or semiconducting type. The dependence of the forbidden gap on the method of synthesis of the specimens[83] and on the presence of a wide variety of impurity centres or crystal defects,[83] in particular vacancies in the metal sublattice, is evident. The possibility of the formation of the latter for CaB_6 has been noted, for example, in the study of the fusion of CaB_6, whereupon dissociation takes place with the preferential evaporation of calcium.[84,85] This finding can be readily accounted for by the specific features of the energy structure of CaB_6, because the bonds between the atoms of the nonmetal sublattice of the boride play a dominant role in the organisation of the inter-species interaction.

Calculations for strontium and barium hexaborides within the framework of the LCAO formal treatment[35] indicate that the structures of their electronic spectra are similar to that for CaB_6 (Fig. 4). Therefore, without going into their details, we shall only note that the form of the valence DOS is determined primarily by the type of the distribution of states in the B_6 groups (Fig. 6) and is characterised by five principal maxima *A*–*E*. Comparison with the data obtained by X-ray emission BK_α spectra of BaB_6 shows (when account is taken of the simplifications used in the calculation)[41] a fairly reasonable agreement between the energies of the principal B 2*p* maxima with the exception of the intense peak *A* manifested on the spectral line in the form of a weak high-energy bulge.

4. Aluminium borides

The phase diagrams for the Al–B system indicate[86–95] the existence of at least two stable binary phases—aluminium diboride AlB_2 and aluminium dodecaboride AlB_{12}. Two possible modifications have been identified for the latter compound—monoclinic and tetragonal.[10] The existence of the AlB_{10} phase,[90–92,95] found by Kuz'ma,[11] was not unambiguously confirmed.

In terms of the aspect under discussion, the most interesting compound is the diboride AlB_2—a phase the structural type of which (or one related to it) is characteristic of a large number of binary and more complex *d* metal borides (see below). Aluminium diboride has one of the simplest structures and contains two alternating networks of atoms—the metal and boron (Fig. 1).

General ideas about the nature of the metal–metal bond in the diborides AlB_2 have been discussed within the framework of the Hückel model.[96,121] It is claimed that the system of chemical bonds in such crystals is based on the M–B and B–B interactions, whereas the M–M interactions (in the direction perpendicular to the network of B atoms) are antibonding.

The band structure of AlB_2 (calculation by the LCAO method)[97] is determined by the presence of filled boron bands (the structure of which is found to be similar to that for graphite) split into states with σ are π symmetries. Part of the charge density is transferred to the latter from the metal atom, whereupon the metal atoms acquire the effective charges +1.884 e (Al) and −0.942 e (B). The B–B bonds have a stabilised π component; the $Alp_{x,y}$ functions are mixed with the band comprising these states, giving rise to the B–Al bond. We may note, however, that in the calculations[97] the basis set did not include the Al 3*d* states, allowance for which (see above) may significantly amend the fine structure of the band in the energy spectrum of the crystals.

Overall, the calculations[97] are in satisfactory agreement with X-ray emission spectroscopic data[98] and have been used to interpret the anisotropy of the electrical properties of AlB_2 (on the basis of the analysis of the topology of the Fermi surface and estimates of the differences between the effective masses of the carriers for different directions in *k* space).

The molecular orbital scheme for the fragment modelling AlB_{12}, for which semiconducting properties have been predicted, has been calculated[99] by the LCAO method in terms of the Gaussian orbital basis set (GO LCAO).

III. Transition *d* metal borides

Transition *d* metal borides constitute one of the most numerous and thoroughly investigated groups of binary boride phases, and numerous monographs and reviews have been devoted to their crystal chemistry and physicochemical properties.[1-14]

The analysis of the possible approaches to the description of the electronic structure and properties of compounds of this type will be begun with the Ti–B system.

1. Titanium borides

Numerous studies have been devoted to phase formation in the Ti–B system.[1-3,5,7,9,11-14] It is suggested that not less than five individual phases exist in the Ti–B system.

Most of the investigations of the electronic properties of the boride phases of titanium refer to titanium mono- and di-borides. However, before turning to the consideration of the results, we shall mention the calculations of the perturbations in the electronic states of titanium when boron atoms are introduced into its interstices (the corresponding region in the binary system with a low content of the nonmetal is designated as the α-phase on the phase diagrams).[100]

The LMTO Green function method (LMTO-GF) has been used[100] in the calculation for the Ti–B system, in which the nonmetal atom was placed at the centre of an octahedral interstice of the face-centred cubic structure of titanium. It follows from the analysis of the distribution of the local density of states (LDOS) of boron that the quasi-core B 2*s* functions form a discrete impurity peak near the lower edge of the valence band of the matrix, while the B 2*p* function overlaps the lower part of the valence band of titanium, promoting the formation of Ti–B bonds.

The perturbing effect of the impurity on the electronic states of the matrix (ΔN) has also been considered. It was established that in the region of energies corresponding to the localisation of the impurity states, two positive $\Delta N(E)$ peaks are observed. The first and second peaks correspond respectively to the states of titanium mixing with the 2*s* and 2*p* orbitals of the interstitial atom respectively.[100] In the pre-Fermi region, a characteristic oscillating $\Delta N(E)$ structure is observed, reflecting the redistribution of the high-energy states of the metal atoms in the vicinity of the interstitial element. Negative values of $\Delta N(E)$ correspond to spectral ranges with a lower electron density $N(E)$ than for pure titanium and conversely. We then have $\Delta N(E_F) > 0$, i.e. the doping of titanium with small amounts of added boron leads to some increase in $N(E_F)$ for the alloy primarily owing to the disturbance of the bond system in the ideal crystal. Nonequivalent Ti–B and Ti–Ti bonds are formed in this case in the vicinity of the impurity *p* centre. Concentration of electron density in the region of energies of the B 2*s* and B 2*p* functions corresponds to bonds of the first type, whilst positive pre-Fermi $\Delta N(E)$ maxima correspond to bonds of the second type.

The next step was to investigate the effect of the interstitial elements on the electronic states of titanium atoms in the face-centred cubic structure constituting the first and second coordination spheres of the impurity atoms.[100] The γ-Fe_4N structure was used as a model.

The total and local DOS of the hypothetical Ti_4B are presented in Fig. 7. In contrast to the isolated impurity, the B 2*s* and B 2*p* states now form bands of finite width. It is especially interesting to emphasise that the LDOS for titanium atoms at nonequivalent (relative to the centre of insertion) sites are markedly different. Thus, whereas the titanium atoms in the closest sphere make appreciable contributions to the subbands of the nonmetallic 2*p* states, the extent of such mixing is smaller for the Ti atoms in the next sphere, which indicates the local character of the Ti–B bond. This is also reflected in the charge and energy states of the crystallographically nonequivalent metal atoms.

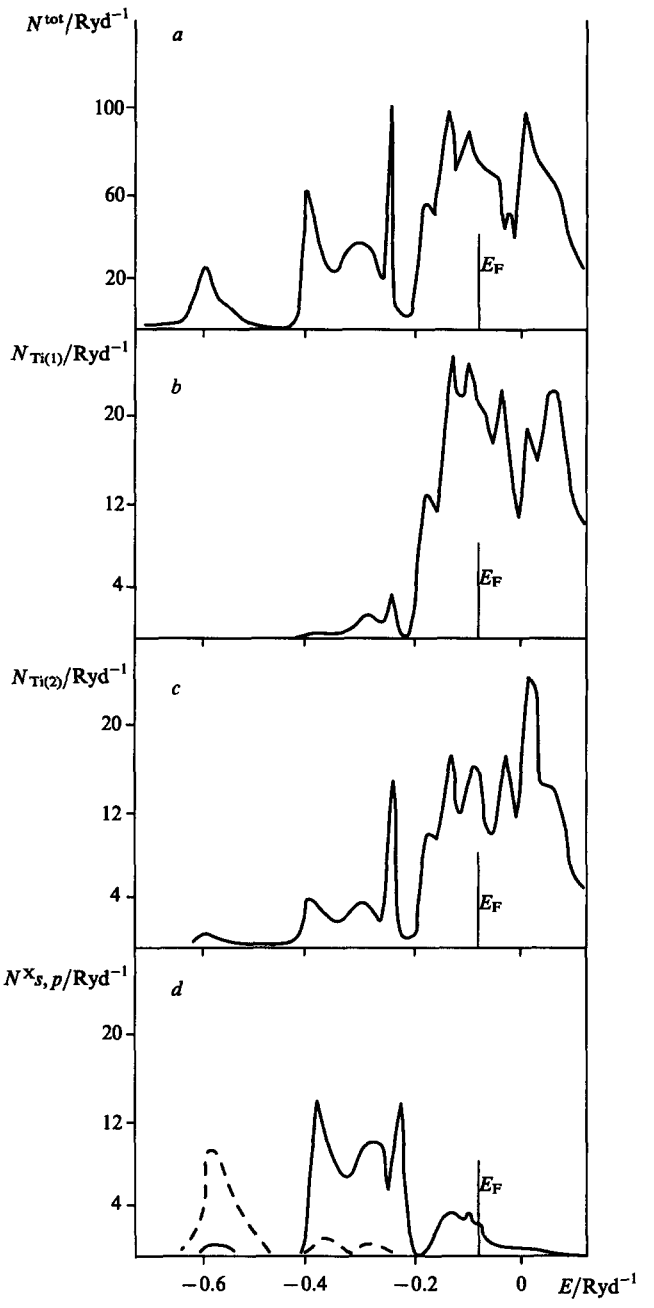


Figure 7. The band structure of Ti_4B (γ-Fe_4N structural type) according to LMTO calculations:[100] (*a*) total density of states; (*b*) and (*c*) LDOS for titanium atoms in the second and first (relative to the nonmetal) spheres; (*d*) densities of B 2*s* (dashed curve) and B 2*p* (continuous curve) states.

Analysis of the valence subbands showed that the maximum contribution to the hybrid Ti_4B band comes from the *d* states of the nearest atoms, i.e. the Ti–B bonds are organised in conformity with the *p*–*d* hybridisation mechanism typical for refractory phases.[101-104] One cannot also neglect the involvement of the *s* and *p* functions of titanium in these interactions. Thus it is mainly the Ti 4*s* functions of the titanium atoms constituting the second metal sphere which enter into the interaction with the nonmetals. In other words, both the energies and the nature of the bonds between the interstitial elements and the titanium atoms in the first and second spheres are different.

These differences in the nature of the Ti–B bonds are reflected in the distribution of the states of the metal band, i.e. lead to the anisotropy of the Ti–Ti bonds.

We may note that the calculated data[100] have been used for a qualitative treatment (in relation to the Ti–B and Ni–B systems) of the phase relations observed on the phase diagrams for metal–boron systems. For this purpose, use was made of the changes in the total energy (ΔE) of the face-centred cubic titanium matrix when a nonmetal atom is introduced into an interstice. These changes were obtained by solving the single-impurity problem by the method proposed by Anisimov et al.[105] It was found that $\Delta E < 0$ for the systems considered, i.e. the introduction of nickel and boron atoms, involved in covalent interactions with the matrix, into the interstices of the face-centred cubic titanium and nickel structures is energetically favourable. However,

$$|\Delta E^{Ti-B}(-0.767\ \text{Ryd})| > |\Delta E^{Ni-B}(-0.673\ \text{Ryd})|\ .$$

In other words, the boron in the octahedral positions in titanium is more strongly bound than in the nickel matrix. This agrees with the known fact that compounds up to the diborides are formed in the Ti–B system, whereas the maximum content of boron in the nickel compound does not exceed Ni/B $\approx$ 1. Naturally, in analysing the results[100] one cannot fail to take into account the direct B–B interactions arising in the boride phases, which should introduce significant corrections to the overall energy relations of the systems under discussion. However, the above data[100] make it possible to gain a general idea about the role of the metal–nonmetal interactions in the boride phases considered.

With increase in boron content, the compound Ti_2B (orthorhombic structure of the Al_2Cu type) was detected on the Ti–B phase diagram. In its structure, all the boron atoms are surrounded by metal atoms.[5,11] The increase in the B/M ratio is accompanied by a further transformation of the electron energy spectra (EES) of the matrix [calculation by the method of augmented spherical waves (ASW)].[106] The B 2*p* states are then mixed in throughout the width of the occupied part of the valence band, which is predominantly of the Ti 3*d*, *s* type. In addition, the valence band contains near its lower edge two subbands of the B 2*s* type separated by a narrow energy gap. The bonds are formed as a result of two types of interactions: Ti–Ti and Ti–B; direct B–B bonds were not detected. The Fermi level is located on the high-energy slope of the intense Ti *d* type DOS peak.

The further genesis of the band structure of titanium boride as the boron content increases will be considered by comparing the EES of the higher borides—TiB and TiB_2.

Titanium monoboride crystallises with a structure of the FeB type.[11] There are also data concerning monoborides crystallising with structures of the NaCl and ZnS types.[7–10] It has likewise been suggested[11] that the cubic monoboride (NaCl structural type) can be obtained either in the form of a high-temperature phase or in the form of a phase stabilised by added carbon.

Calculations for the orthorhombic TiB have been carried out.[107–109] The dispersion of the bands and the total density of states (TDOS) in TiB have been investigated[107] by the nonself-consistent LCAO method in the tight binding approximation.[35,110] A broadening of the dispersion in the k_z direction ($\Gamma-Z$, $T-Y$, $R-S$, $U-X$) compared with k_x and k_y was noted. This should indicate the predominance of the bonding effects along the *c* axis of the crystal, along which the chains of boron atoms are oriented, i.e. a pronounced cohesion anisotropy. The TDOS in TiB comprises (in order of decreasing binding energy) the B 2*s*, B 2*p*, and Ti *d*, *s* states (Fig. 8). The Fermi level is located at the DOS minimum in the vicinity of the intense virtual *d* type resonance. Calculations of the populations of the atomic orbitals made it possible to estimate the charge states of titanium (−1.31 e) and boron (+1.31 e).

The bond indices of various atoms, forming layers in the TiB crystals, have been calculated[107] in the cluster approximation by the method proposed by Bell and Perkins.[111] The calculation was carried out taking into account all the interacting neighbours in accordance with the Born–Carman principle.

The results show that the B–B covalent bonds are most highly populated.[107] In the calculations of the bond indices in other similar

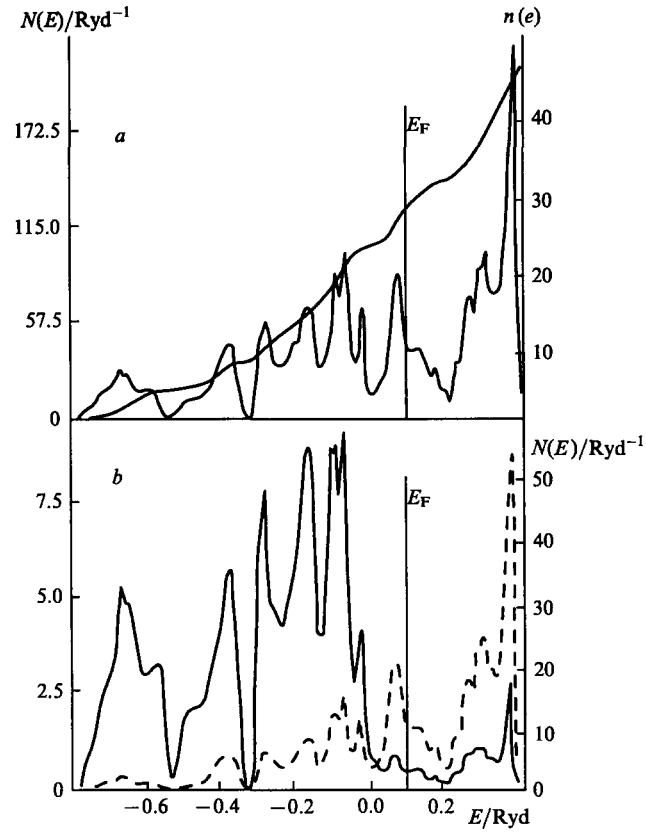


Figure 8. The total (*a*) and local (*b*) densities of states in TiB (FeB structural type). Calculation by the LMTO method.[109]

TiB clusters, where the lowest unoccupied levels lying 0.01 and 0.1 eV above E_F (this simulated the thermal excitation of the boride) were filled, the bond indices of the B–B and Ti–B types remained virtually unchanged, but the index of the Ti–Ti type diminished significantly. Consequently, heating of the specimens affects primarily the bond system in the metal sublattice of the boride.

Calculations for TiB using the more accurate self-consistent augmented spherical waves method[112,113] have been performed.[108] Here a study was made of the structural stability of 3*d* metal monoborides for five possible crystallographic modifications (structures of the FeB, CrB, NaCl, CsCl, and CuAu types). For this purpose, the total crystal lattice energies were calculated for the six cell volumes differing by ±15% from the equilibrium value in the case of all the structures listed above (Fig. 9). Evidently, in conformity with experiment, the orthorhombic modification is energetically most favourable for the boride under discussion, while the CsCl and CuAu structural types are least likely; an intermediate value was obtained for the NaCl type. The equilibrium volume of the TiB unit cell was reasonably well produced and the volume modulus of elasticity was calculated (Table 1).

Table 1. Theoretical (I)[108] and experimental (II)[114–116] unit cell volumes *v*, atomic magnetic moments μ, and volume moduli *b* of titanium monoboride.

Compound	v/Å^3		μ/μ_B		*b*/kbar
	I	II	I	II	
ScB	25.6	—	0	—	3100
TiB	22.6	21.3	0	0	2400
VB	19.5	18.8	0	0	2800
CrB	18.0	17.1	0	0	3400
MnB	17.3	17.2	2.00	1.83	2600
FeB	16.8	16.4	1.25	1.12	2500

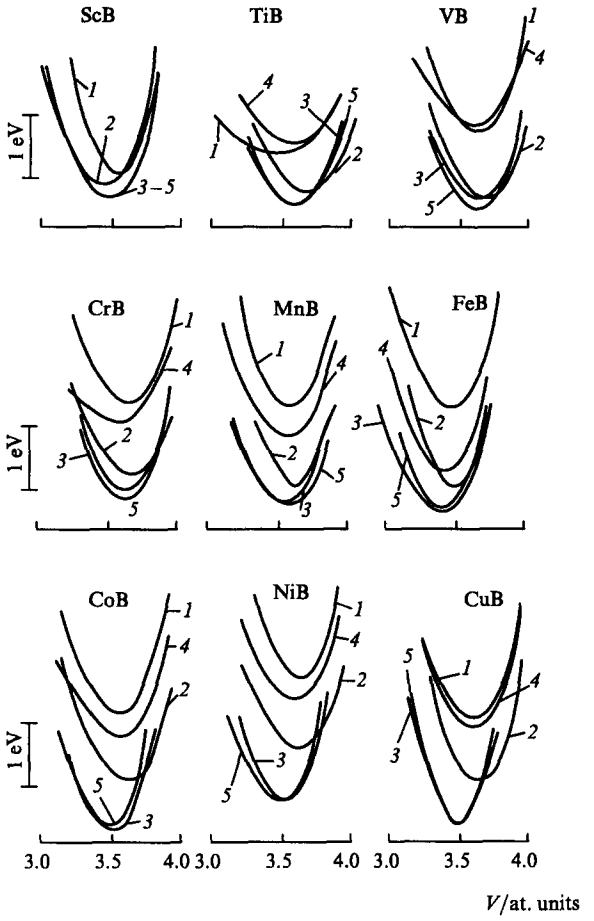


Figure 9. Variation of the total one-electron energy of 3*d* metal borides as a function of the crystal structure of the phase and the volume of the unit cell (calculation by the ASW method).[108] Type of structure: (*1*) CuAu; (*2*) NaCl; (*3*) FeB; (*4*) CsCl; (*5*) CrB.

A somewhat different approach to the discussion of the relative stabilities of the structural modifications of TiB, based on the calculations of the band spectrum of the crystals, has been used in a study[109] where the calculation for TiB with structures of the NaCl and FeB types was carried out by the LMTO method in the atomic spheres approximation in terms of the formal treatment of Sabiryanov et al.[117]

A multipeak TDOS structure was obtained for the orthorhombic monoboride TiB (FeB structural type) (Fig. 8). Taking into account the decomposition of the TDOS into atomic components, one can segregate arbitrarily two low-energy bands, predominantly of the B *s* and B *p* types, separated by a narrow forbidden gap from the band with an energy lower by approximately −3.14 to −0.1 Ryd than E_F and having a mixed $p-d$ character. The intense resonance of the Ti *d* and Ti *s* states in the vicinity of the Fermi level is also noteworthy. A significant difference between the results of the calculation by the self-consistent LMTO method[109] and the data of Armstrong and Perkins[107] concerns the position of the lowest unoccupied *d* band, which is separated from E_F by a deep DOS minimum according to Sabiryanov and Ivanovskii[109] (Fig. 8).

The DOS of the cubic monoboride (NaCl structural type)[117-119] differs significantly from that examined above for the orthorhombic TiB (FeB type). It has a two-band form[101-104] characteristic of NaCl-like phases (carbides, nitrides, etc.) with a distinct separation of the bands of the B 2*s* and B 2*p* states. Adjustment for self-consistency[119] then leads to the appearance of a forbidden gap between the bands, whereas in the absence of such adjustment their overlap is observed.[118]

We shall now analyse the energy relations of the paired bonds (E_b) in TiB (with structures of the FeB and NaCl type) using the method described by Sabiryanov et al.[117] The energies E_b for the orthorhombic borides are listed in Table 2. Evidently the interactions between boron atoms located in the closest layers of the crystal make the greatest contribution to the energy of the covalent bonds. This result differs fundamentally from the conclusions reached by Armstrong and Perkins,[107] who postulate that the interaction between boron atoms located in one layer predominates. Evidently, the analysis of the cohesive properties of crystals, based solely on the calculations of the parameters of the overlap of wave functions,[107] may not be always correct.

Table 2. Pair energies of the covalent bond in titanium borides.[102]

Pair	Energy of covalent bond/mRyd	Pair	Energy of covalent bond/mRyd
TiB (NaCl)		**TiB (FeB)**	
Ti(1)–Ti(1)[a]	−56.16	Ti(3)–Ti(2)	−33.18
Ti(1)–B(2)	−674.04	Ti(3)–Ti(3)[a]	−15.06
B(2)–B(2)[a]	8.12	Ti(3)–Ti(3)[b]	−98.92
		Ti(3)–Ti(1)	−210.14
TiB_2		B(7)–Ti(1)	−341.74
Ti(1)–B(2)	−350.40	B(7)–Ti(2)	−246.22
Ti(1)–Ti(1)[a]	−21.14	B(7)–Ti(4)[a]	−48.70
Ti(1)–Ti(1)[b]	−95.02	B(7)–Ti(3)	−212.00
B(2)–B(3)	−975.42	B(7)–B(8)	−705.40

[a] Atom from the cell displaced by unit translation vector along the *a* axis.
[b] Atom from the cell displaced by unit translation vector along the *c* axis.

In conclusion, we may note that the total covalent interaction energy is 1887.9 mRyd for the cubic boride and 1907.1 mRyd for the orthorhombic boride,[109] which indicates unambiguously the greater stability of the orthorhombic phase and is fully consistent with the conclusions reached by Mohn and Pettifor.[108]

Proceeding now to the consideration of the energy spectra of the higher titanium boride TiB_2 (AlB_2 structural type), we may note the calculation for the diboride[120] carried out by the LCAO cluster method in the tight binding approximation[18] as one of the first approximate calculations. The calculations were performed for a lattice fragment (with D_{3h} symmetry) taking into account the fourth- and fifth-order neighbours in terms of a basis set comprising the B *s*, *p* and Ti *s*, *p*, *d* orbitals. The resolution of the resulting molecular orbitals into atomic contributions makes it possible to estimate the width of the TiB_2 valence band (~13.56 eV), the lower edge of which is made up mainly of the *s* and *p* states of boron with progressively increasing contributions by the Ti *s* orbital as the energy of the molecular level decreases. Analysis of the parameters of the electronic structure of TiB_2, calculated by Samsonov et al.,[120] indicates the Ti → B charge transfer as additional p_x states of boron are filled. The latter form B–B bonds both within planes (π-bonds) and between layers (σ-bonds), the maximum filling of the p_x states (in the TiB_2–VB_2–CrB_2 series) being responsible, according to Samsonov et al.,[120] for the extrema in the melting point, the coefficient of thermal expansion, the microhardness, and the phonon component of the thermal conductivity.

Band calculations for TiB_2 have been carried out by the LCAO method[26] in terms of Hückel's formal scheme,[121] the augmented spherical wave method,[37] and the LMTO method.[109,122] The electron energy spectrum of the diborides has been investigated by spectroscopic methods.[42-46] The $E(\vec{k})$ dispersion relations for TiB_2 have a number of characteristic features compared with the monoborides (Fig. 10). There is no forbidden gap between B 2*s* and the hybrid B 2*s*, B 2*p*, and Ti *d*, *s* bands and there are random degeneracy points in the vicinity of E_F in the $\Gamma-K$, $K-M$, and

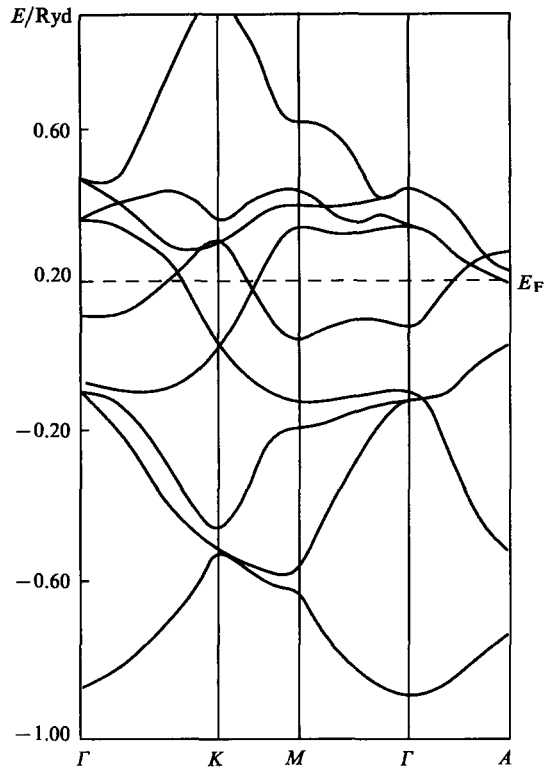


Figure 10. The band structure of TiB_2.[109]

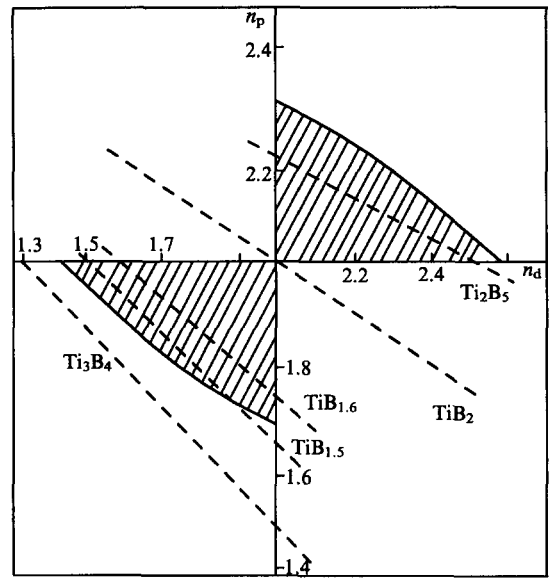


Figure 11. Phase diagram for the compound TiB_x. The regions of possible superconductivity are shown cross-hatched.

$\Gamma - A$ directions. Three principal subbands, made up of the B 2*s* state, the B 2*s*, 2*p* and Ti *d*, *s* states, and the Ti *d*, *s* states respectively, can be differentiated in the TiB_2 valence band. The Fermi level is located in a deep DOS minimum separating the valence and conduction bands, which agrees well with the results of X-ray emission analysis.[41]

Analysis of the energy relations of the paired bonds (Table 2) shows that the interaction between the boron atoms located in one plane (network) is most significant whereas bonds between networks were not detected. The next in magnitude is a type Ti–B interaction, the Ti–Ti bond energy being an order of magnitude smaller. The results of calculations of the partial energies of the pair interactions proved somewhat unexpected.[109] According to these calculations, the Ti 4*p*–B 2*p* (72 mRyd) and Ti 4*p*–B 3*s* (66 mRyd) bond energies are comparable to the Ti 3*d*–B 2*p* (92 mRyd) bond energy.

Estimates of the charge polarisation,[120,122] indicating a displacement of the electron density to the nonmetal atoms, are consistent with experimental X-ray diffraction data.[123]

The possibility of the appearance of high-temperature superconductivity in layered titanium borides has been examined[124] on the basis of the generalised Hubbard–Emery model[125,126] (taking into account the integrals of the jumps between nearest neighbours). The presence in such borides of separated $d_{xz,yz}$ states, tunnelling through boron ions in the degenerate $p_{x,y}$ states, has been postulated. Calculations of the amplitude of the kinematic interaction (by Dyson's method) taking into account the possible filling of the bands for the hexagonal TiB_x phases showed that superconductivity can occur in the composition range $TiB_{26/17}$–TiB_2 (Fig. 11). The conclusions reached by Zaitsev[124] agree qualitatively with the results of other studies,[127,128] in which the possibility of superconductivity in the $TiB_{1.5-1.6}$ phases and its absence in the TiB_2 and Ti_3B_4 phases was indicated.

The quantitative microscopic description of the parameters of the superconducting state of the borides undoubtedly requires special consideration.

2. 3*d* Metal borides

Proceeding now to the discussion of the electronic properties of the borides of other 3*d* metals, we may note that the boride phases formed by specific 3*d* metals have been investigated to significantly different extents. Systematic calculations have been performed only for the hemiborides[106] and monoborides.[108] It follows from them that the dispersion relations and the energy distributions for these phases are similar to those for Ti_2B and TiB (see above), provided that account has been taken of the increase in the filling of the *d* bands as a function of the concentration of the valence electrons (CVE) and of the consistent low-energy shift of the metallic subbands with increase in the atomic number of the transition metal along the Period.

Most studies carried out hitherto have been devoted to the description of the characteristic features of the electronic structures of iron and nickel borides. We shall consider in greater detail their principal results.

The hemiboride Fe_2B and the monoboride FeB have been differentiated in the Fe–B system as equilibrium phases.[1,2,9,11]

The hemiboride has a body-centred tetragonal structure of the Al_2Cu type ($a = b = 4.249$ Å, $c = 5.110$ Å, space group *I4/mcm*), where the boron atoms are located between layers of iron atoms.[11] Iron monoboride crystallises with formation of an orthorhombic structure in which there are four molecules in the unit cell.[1]

The spectroscopic properties of iron borides have been investigated.[43–45,54] The results of numerical quantum-chemical calculations for Fe_2B and FeB have been published.[106,108,129–131]

One of the most complete calculations of the electron energy spectra of Fe_2B has been carried out[131] by the linearised APW-(LAPW) method, in which the energies of the core electrons were calculated in accordance with the full relativistic Dirac–Slater scheme. A semirelativistic approach, taking into account the contributions to the Dirac equation of the Darvin and mass–velocity terms, was used to calculate the energy of the valence electrons. In the solution, account was taken of plane waves (~270) with energies of up to 6.15 Ryd and angular momenta $l \leqslant 8$. Adjustment for self-consistency (with respect to energies) was carried out until the attainment of the condition $\Delta E \leqslant 4$ mRyd.

Analysis of the dispersion curves and of the total and partial densities of states in Fe_2B shows that the bands due to the B 2*s* and B 2*p* states lie below the partially filled Fe 2*s* states. Two lowest bands are made up of 2*s* states of two boron atoms in a unit cell.

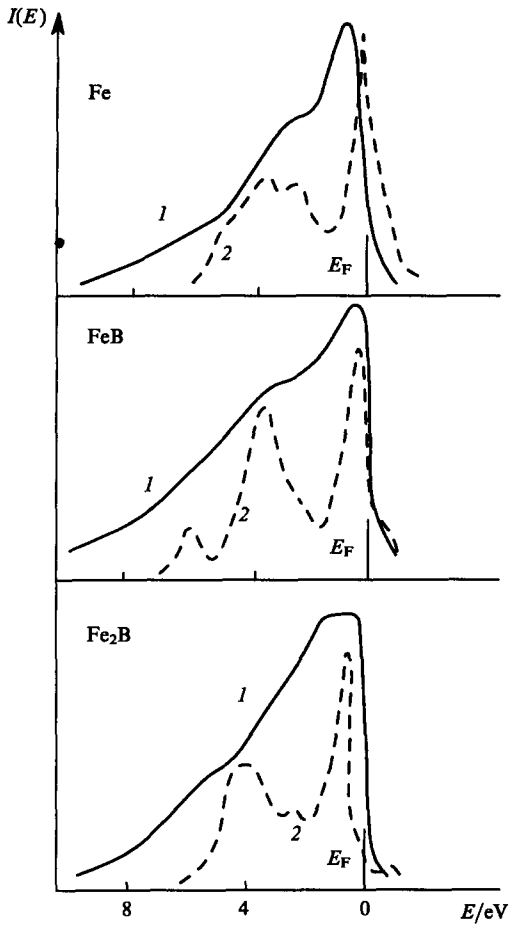


Figure 12. Fe 3*d* electron spectra (curves *1*) and densities of Fe 3*d* states (curves *2*) in Fe, Fe_2B, and FeB.

The degenerate B *p* states are located in the range −0.6 to 0.2 Ryd. An appreciable superposition of the iron and boron states occurs higher along the energy scale. Finally, the highest energy peak reflects the concentration of the bonding Fe 3*d* orbitals, while a further two resonances, corresponding to the nonbonding Fe 3*d* states, are observed in the immediate vicinity of E_F.

Comparison of the DOS and the photoelectron spectra of Fe_2B (Fig. 12) shows that they are acceptably consistent with one another.[131] Evidently the Fermi level coincides with the local Fe 3*d* resonance band, where the DOS (calculated per iron atom) reaches ~1 Ryd^{-1}. If account is taken of the fact that the Stoner parameter *I* (for pure iron) is ~0.92, it becomes evident[131] that, since $IN(E_F) \gg 1$, the manifestation of ferromagnetic properties is to be expected for Fe_2B. Unfortunately the calculations[131] were performed solely in the spin-limited variant, which made it impossible for the authors to estimate the atomic magnetic moments.

Table 3. Distribution of valence electrons among the MT spheres of Fe_2B and FeB (calculated by the LAPW method).[131]

Compound	Type of sphere	Number of electrons		
		s	*p*	*d*
Fe_2B	Fe	0.3205	0.3907	6.0726
	B	0.3654	0.6329	0.0161
FeB	Fe	0.2973	0.4027	6.1631
	B	0.3667	0.6785	0.0171

Analysis of the interatomic bonds in Fe_2B, based on the calculation of the distribution of states in the MT spheres (Table 3) and charge density maps [in the (120) plane] for the boride leads to the conclusion that there is significant B 2*p*–Fe 3*d* hybridisation between the boron atoms and the eight nearest iron atoms. Thus the charge density contours indicate the concentration of charge density along the B–Fe line and also between the nonmetallic centres, which is evidence for the existence of direct B–B bonds.

We may also note that charge transfer between the iron atoms in the hemiboride was not observed.[131] The formation of direct covalent Fe–B and B–B bonds enhances the cohesive properties of Fe_2B compared with Fe.[131]

Direct calculations of the Fe_2B core orbital energies (Table 4) and of electron densities on the iron nuclei, which have been used to calculate the isomeric shifts (measured by Mössbauer spectroscopy), are of interest.

The spin-labelled LAPW calculation for FeB has been performed by the method described above. The boron 2*s* states are concentrated in the vicinity of the bottom of the valence band. The higher-energy *A* and *B* maxima correspond to the hybridised Fe 3*d*–B 2*s* states, whereas in the vicinity of the Fermi level predominantly the Fe 3*d* functions make the main contribution to the DOS (Fig. 13). Comparison of the results of the calculation with emission spectroscopic data[61–63] shows that they are in agreement.

The formation of covalent bonds (as a result of *sp*–*sp* hybridisation) between boron atoms constituting the linear chains is characteristic of iron monoboride as well as Fe_2B. Charge transfer between the iron and boron atoms in FeB has not been observed (Table 3). It is seen from the data presented in Table 4 that the calculation in the study of Joyner et al.[131] correctly reproduced the sequence of the energies of the core levels of FeB, which are somewhat displaced in the direction towards E_F relative to the experimental results.[62,63] We may note that, following the transition $Fe_2B \rightarrow FeB$, the energy relations for these levels remains virtually unchanged (within the limits of ±0.1 eV), which is also consistent with experiment. The Fe_2B and FeB valence band schemes are presented in Fig. 14.

Table 4. The energies (Ryd) of the core levels of Fe_2B and FeB.

Compound	Fe 2*s*[a]	Fe $2p_{1/2}$	Fe $2p_{3/2}$	Fe 3*s*	Fe $3p_{1/2}$	Fe $3p_{1/2}$	B 1*s*
Calculated data[131]							
Fe_2B	−59.588	−51.385	−50.471	−6.348	−3.951	−3.837	−12.432
FeB	−59.584	−51.384	−50.469	−6.338	−3.960	−3.846	−12.352
Experimental data[61,63,66]							
Fe	−62.14	−52.94	−51.98	−6.71	−3.90	—	−13.83
Fe_2B	−62.11	−52.96	−51.99	−6.74	−3.90	—	−13.82
FeB	−62.14	−52.96	−52.00	−6.74	−3.92	—	−13.82
B	—	—	—	—	—	—	—

[a] The energies are quoted relative to the Fermi level.

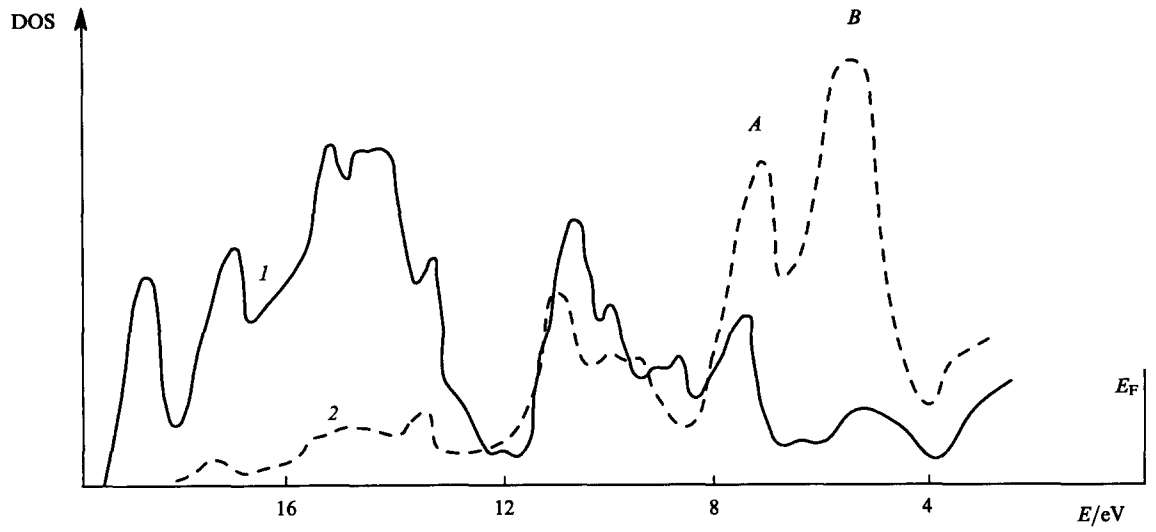


Figure 13. The local densities of B 2*s* (curve *1*) and B 2*p* (curve *2*) states in FeB.[131]

The energy structure of nickel monoboride (type CrB structure)[11] has been calculated[106] by the ASW method (Fig. 15). The relative positions of the total and local DOS make it possible to differentiate the sections of the electronic state spectrum corresponding to the $p-p$ bonds in the chains of metalloid atoms (peak *A*), to the Ni – B interactions (peaks *B* and *B'*), and to nonbonding $d-d$ states (peak *C*). The calculated value of the volume modulus [of elasticity] and of the unit cell volume are presented in Table 2.

The value of $N(E_F)$ for crystalline NiB is not quoted in Mohn's study,[106] although it is seen from Fig. 15 that it is insignificant and is much smaller than for manganese and iron monoborides. Measurements of magnetic susceptibility made it possible to assign NiB to the class of weak paramagnetic materials and to estimate $N(E_F) \approx 0.18$ state eV^{-1} $atom^{-1}$,[132,133] in which the contributions of the *s* and *p* states predominate.

The parametrised LCAO method with the Slater–Coster (SC) tight binding approximation has been used[134] in calculations for the lowest nickel boride Ni_3B (Fe_3C structural type).

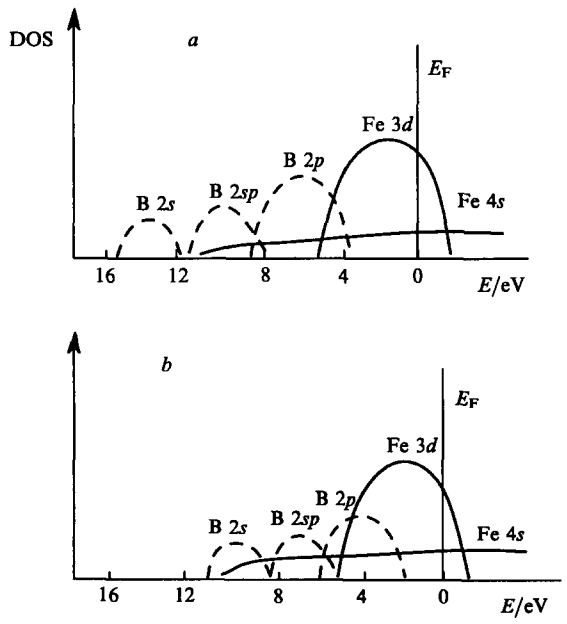


Figure 14. Schematic illustrations of the structures of the valence bands of FeB (*a*) and Fe_2B (*b*).

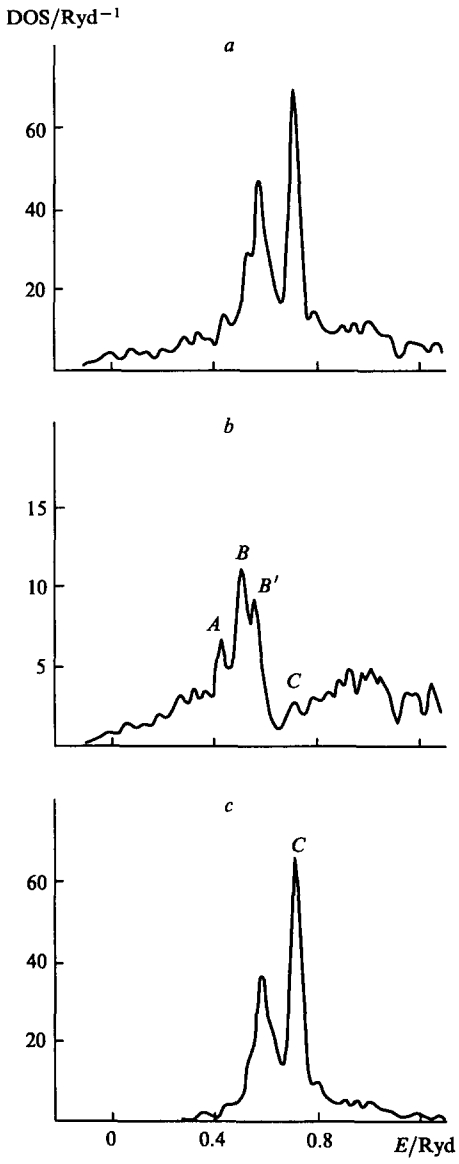


Figure 15. The total (*a*) and partial densities of B 2*p* (*b*) and Ni 3*d* (*c*) states in NiB.

The *B* 2*s*, B 2*p*, and Ni 3*d* functions were included in the basis set and account was taken of the interaction of only the nearest neighbours. The SC parameters for the Ni–Ni bond were taken from calculations performed for metallic nickel,[135,136] while the parameters of the B–B bond were obtained by extrapolating the SC parameters for carbon.[134]

The energy spectrum of the valence electrons of Ni_3B is typical of binary borides and contains two lowest bands (E = 0.0315 and 0.0607 Ryd) made up of B 2*s* states. The following twelve bands (0.433–0.569 Ryd) reflect the hybrid Ni 3*d*–B 2*p* states, the upper band having predominantly the *d* character. The higher energy free bands ($E \geqslant 1.135$ Ryd) also have a mixed B 2*p*–Ni *d*, *s* character.

The band structure in the vicinity of E_F makes it possible to assign Ni_3B to the class of paramagnetic materials, which is consistent with the available experimental data.[138,139]

3. 4*d* Metal borides

Proceeding now to the discussion of 4*d* metal borides, we may note that the energy structure of these compounds has been investigated in much less detail than that of the 3*d* analogues. Zirconium diboride, which has a series of valuable physicochemical properties, namely a high melting point, high electrical and thermal conductivities, and a high hardness, has attracted most attention hitherto.[1–4,8–11] This makes it possible to employ it as a cathodic material, as an abrasive, and as a component of heat-resistant alloys, composite materials, etc.

Nonself-consistent calculation for ZrB_2 by the APW method using the exchange potentials specified by Slater and Kohn-Shem[140] showed that the density of states in ZrB_2 is defined by three characteristic maxima. The first is linked genetically to the bands of the B 2*s* states, while the next two correspond to the 2*p* states of the nonmetal.

The ZrB_2 band structure has been investigated[141] by the self-consistent Korringa–Kohn–Rostoker (KKR) method in terms of the MT spheres approximation. The initial potential was determined by the Mattheiss method[142] with the initial atomic configurations Zr $4d^{2.5}5s^{1.5}$ and B $2s^22p^1$. The exchange-correlation parameters α were taken from Schwarz,[143] whilst the remaining parameters were taken from Ham and Segal[144] and Segal.[145] Adjustment for self-consistency proved most critical in relation to the energies of a series of virtual DOS peaks and the distribution of the Zr *d* electrons. Their number in the MT sphere of the metal (compared with the nonself-consistent calculation) increased by ~0.667 e.

The dispersion $E(k)$ proved extremely complex, which hindered a clear interpretation of the nature of the interatomic bonding. In describing the structure of the energy bands, Johnson et al.[141] confine themselves to only several preliminary remarks. In particular, it is noted that the lowest bands (T_1, T_4, Z_1, Z_4) resemble the sp^2 σ-bonding states in graphite[146] and can be made up of the bonding states of boron (s, p_x, p_y). Nevertheless, one cannot fail to take into account the admixture of metal functions in this region.

By analogy with 'two-dimensional' graphite, it is suggested that the band intersecting the Fermi level (T_1) is associated with the π band of boron, while the lowest unoccupied Σ_3 and all the s_4 bands are made up of the antibonding B π states significantly hybridised with the Zr *d* orbitals. A detailed analysis of the remaining states has been carried out by Johnson et al.,[141] who examined also the principal differences between the energy structure of ZrB_2 and the intercalated layered phases of the KC_8 and LiC_8 types.[147,148] They also analysed the composition of the orbitals forming the pre-Fermi region — the predominance of the Zr *d* states was noted.

The results of the calculation[141] were also used for the theoretical interpretation of the optical properties of zirconium diboride. Fig. 16 presents the imaginary part of the relative permittivity of the ZrB_2 film[149] and the calculated curve (calculated on the hypothesis of constant matrix elements).

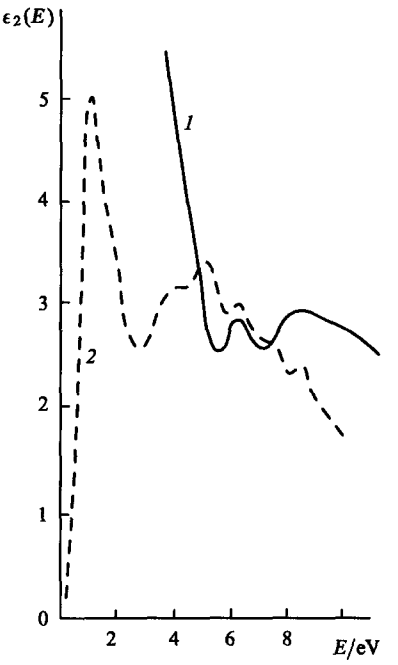


Figure 16. The energy dependence of the dielectric function for ZrB_2:[141] (*1*) experiment; (*2*) calculation.

Evidently, within the framework of the approximations adopted, the most reasonable description of the relative permittivity is attained in the range 6–7 eV. Its variation in the given energy range may be correlated with the transitions between sets of one-electron band states located directly above and below the Fermi level.

The melting point of ZrB_2 has been estimated[141] (from the Lindemann equation).[150] It was noted that the high melting point $T_m \approx 3000$ °C is due primarily to the significant covalent Zr–B interactions.

A fairly good agreement has also been observed between the quantity $N(E_F) = 0.20$, calculated using the low-temperature heat capacity γ data, and the values obtained in calculations:[141] 0.31 eV (nonself-consistent calculation) and 0.26 eV (self-consistent calculation) per unit cell. In conclusion, we may note that the results of the above study[141] have also been used for the qualitative interpretation of the X-ray electron spectra, the Hall effect, the conductivity, and the ^{11}B NMR spectra of the diboride. As regards the problem of charge transfer in ZrB_2, the data obtained permit the claim that there is partial charge polarisation in the crystal in the B → Zr direction.

The remaining 4*d* metal borides have been investigated to a much lesser extent or not at all. Among the available results, we may note the LMTO calculations for the hypo-thetical cubic ZrB,[118,119] in relation to which the problem of the effect of point defects — zirconium and boron vacan-cies — on the spectrum of the monoboride (calculations by the LMTO-GF method) was considered. The marked *s*-type resonance in the region of the minimum in the DOS for the matrix between the *p*, *d* and *d*-like bands of two additional low-energy peaks (in the region of the *s* and *p*–*d* bands of the boride) was established on the LDOS distribution curve of the B defect.[151] Their appearance may be accounted for (by analogy with the similar effects in non-stoichiometric carbides and nitrides)[103] by the increase in the energy of a series of Zr 4*d* states (on dissociation of some of the Zr–B bonds) with appearance of 'lateral' Zr–Zr interactions, which is manifested in the ZrB_x spectrum by the 'vacancy' resonances already mentioned.

The behaviour of $\Delta N(E)$ (the change in the electronic states of the matrix under the influence of vacancies) (Fig. 17) reflects the electronic processes accompanying the removal of a boron atom:

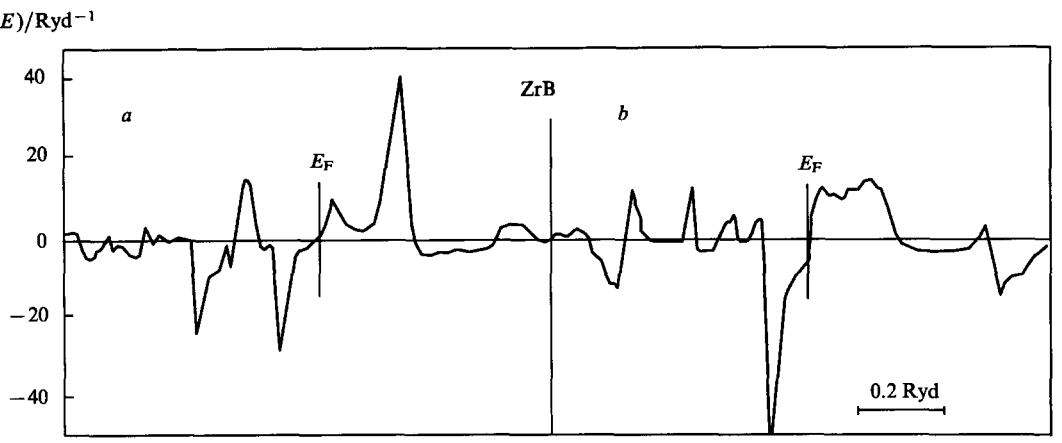


Figure 17. Variation of the density of states in ZrB following the introduction of B (*a*) and Zr (*b*) vacancies.[151]

negative values of $\Delta N(E)$ predominate in the region of the $p-d$ band of the valence band. In other words, the overall DOS of the nonmetallic band of the nonmetal-deficient phase decreases both as a result of the subtraction of the p states of the boron atoms removed and as a result of the transition of some of the d states of the metal to a higher-energy state. This is indicated by the positive $\Delta N(E)$ resonances in the pre-Fermi region (the region of the Zr–Zr bonds).

The nature of the states of the vacancies in the metal sublattice proved to be generally similar.[151] The 'vacancy peaks' are in this case caused by the subtraction of some of the B s,p states ('ruptured B–Zr bonds'), by the increase in their energy, and by a transition to a nonbonding state. The concentration of additional electron density is observed in this range (near E_F).

Estimates of the change in the one-electron energy of the system ΔE in the presence of boron of zirconium vacancies (by the method developed in the study of Ivanovskii et al.[103]) showed that $\Delta E(\text{Zr}) = 0.459$ Ryd and $\Delta E(\text{B}) = 0.508$ Ryd,[131] i.e. $\Delta E(\text{Zr}) < \Delta E(\text{B})$, which reflects the specific features of the bonding in borides. Indeed, the formation of Zr vacancies requires the rupture of only six nearest Zr–B bonds, whereas the formation of boron vacancies presupposes the dissociation of a further twelve B–B bonds. This is the reason why the formation of metallic defects is relatively favoured on energy grounds and in the general case ensures the possibility of the existence in the system of boron-rich phases (up to dodecaborides).[11]

With increase in the atomic number of the 4*d* metal, the ratio $x = \text{B/M}$ diminishes sharply and does not exceed $x = 1/3$ in the case of palladium for example. This fact can be qualitatively attributed to the destabilisation of the structures of the higher borides of the metals at the end of the 4*d* series, while the increase in the CVE leads to a progressive filling of the band of the antibonding *s* and *d* functions of the metal. This can be clearly traced by comparing the ZrB_2 (see above) and TcB_2 band structures.[152]

The energy structure of the hexagonal TcB_2 (space group $P4/mnc$, $a = 2.892$ Å and $c = 7.453$ Å)[153,154] has been calculated[152] in terms of the approximate Hoffmann scheme[155] and a basis set comprising Bloch functions including the B 2*s*, 2*p* and Tc 4*d*, 5*s*, 5*p* orbitals. The number of unit cells for which account was taken of the interaction with the 'central' cell was 2024.

In the analysis of this dispersion of the TcB_2 bands along certain symmetrical directions of the Brillouin band, the compact group of bands, made up of Tc 4*d* states, in the range −5 to 10 eV is striking. According to Armstrong,[152] this determines the conducting properties of the phase. At the same time the $k_{x,y}$ components of the wave vectors form fairly broad (in terms of energy) $\Gamma-M$, $\Gamma-K$, $A-H$, and $A-L$ bands.

The Fermi level has an energy of about −7.5 eV and is located in the region of *d* resonance. The most distinct pre-Fermi valence band maxima with energies of −8.0, −8.6, and −10.3 eV are also generated by the *d* functions of the metal. Charge transfer takes place in the Tc → B direction and reaches 0.87 e per boron atom, the electronic configuration of boron assuming the form $s^{1.30}p_\sigma^{1.61}p_\pi^{0.96}$.

The nature of the Tc–B bonds may be inferred from the composition of the occupied levels, the decomposition of which into orbital contributions has been examined for the point k with the coordinates 1/3, 3/9, and 1/4 (Table 5). Thus, whereas the four lowest levels mainly include the boron functions and

Table 5. The Mulliken populations (in %) of the occupied TcB levels.[152]

Level	E/eV	B s	B p_σ	B p_π	Tc s	Tc p	Tc d_σ	Tc d_π
1	−18.68	54	39	3	1	0	1	2
2	−18.58	57	34	0	4	0	2	2
3	−14.20	26	62	0	2	0	8	2
4	−13.84	21	62	2	1	0	2	12
5	−12.16	18	7	40	8	0	23	4
6	−11.70	5	60	3	0	0	14	19
7	−11.50	2	65	10	3	0	17	14
8	−10.65	0	15	40	1	0	43	2
9	−10.32	1	10	35	2	0	8	44
10	−9.85	0	8	26	0	0	10	56
11	−8.63	0	5	4	0	1	38	51
12	−8.30	1	3	6	2	5	80	2
13	−7.61	0	14	2	2	1	49	32

the three highest the technetium functions, the middle (5–10) are of a mixed type and indicate the hybridisation of the corresponding states.

Finally a qualitative conclusion about the energy of the Tc–B bonds can be reached by comparing the total energies of the boride and of the initial components.[152] Judging from the data presented, the stabilising role in the formation of technetium diborides can be attributed precisely to the bonds noted above.

4. 5*d* Metal borides

The available information about the electronic structure of binary 5*d* metal borides is extremely limited. A LMTO calculation for the hypothetical cubic HfB (NaCl structural type) has been carried out;[119] the charges on the MT spheres were analysed for a qualitative description of the nature of the interatomic bonds.

The bands of the hexagonal ReB_2 (a = 2.900 Å, c = 7.478 Å) have been calculated[152] by Hoffman's method.[155] The $E(k)$ relation is on the whole a repetition of that for the isostructural and isoelectronic TcB_2. Fundamental differences are not observed also for the TDOS. One may note only a closer disposition in terms of energy of the principal Re 5*d*-like maxima (−9.0, −9.8, and −10.3 eV), a smaller charge transfer from Re to B (0.44 e), and some differences between the atomic configurations of boron ($B\ s^{1.26}p_\sigma^{1.38}p_\pi^{0.79}$).

For the analysis of the role of individual components (B and Re) in the formation of the overall band structure, calculations were performed for the hypothetical 'Re' and 'B_2' crystals with the ReB_2 structure.[152] A system of bands, concentrated in a narrow energy range, was obtained for 'Re'. On the other hand, the dispersion of the bands of 'Re' and 'B_2' with the energy structure of the real boride indicates a greater dispersion of the states of the latter, which is associated with the 'inclusion' of the direct Re–B interaction.

The analysis of the composition of the occupied Re_2B levels, carried out[152] by analogy with that described previously, and calculation of the total energy of the boride make it possible to postulate that the Re–B interactions are important in the stabilisation of the ReB_2 lattice.

The data on the electronic structure of osmium and iridium borides are limited at the present time to those of the study of Novikov et al.,[156] in which the Os_3B_{14} fragment was used within the framework of the nonself-consistent X_α-DV method in the calculation for the $OsB_{1.2}$ phase (hexagonal system, WC structural type). A calculation was performed for a cluster of a similar composition in the case of the hypothetical hexagonal iridium boride. It was established that, in contrast to the isostructural molybdenum and tungsten borides in which the M–C bond predominates, the (Os, Ir)–B interaction is antibonding and the interatomic interactions are based on the B–B bonds, the populations of which are smaller for 'IrB' (~9.04) than for 'OsB' (~11.63). The stability of the structures of the borides has been attributed[156] to this fact: in contrast to osmium boride, iridium boride with the WC structure has been obtained only in the form of the high-temperature modification.[9]

IV. Metal–nonmetal–boron ternary systems

Together with binary systems, ternary and more complex compounds and solid solutions constitute an extensive group of boron-containing phases. The crystallographic and certain physicochemical properties of these systems have been investigated in fair detail.[1,2,5–11] However, the general microscopic models of the conditions governing their formation, stability, the nature of chemical bonding, and properties, based on the results of quantum-chemical calculations, are lacking at the present time. The principal results of the studies of the electronic properties of ternary borides will be examined below within the framework of theoretical and experimental approaches.

1. The M–B–C systems

Studies on the interactions of metal borides with carbon demonstrated that continuous solid solutions (SS) are as a rule not formed in the M–B–C systems (where M is a metal).[157–166] The reasons for this are the significant differences between the atomic radii of boron and carbon and also between their energy characteristics.[157,158] Thus the products of the reactions of Group IV and V metals with boron and carbon are as a rule mixtures of boride, carbide, and borocarbide phases. Their structures, compositions, and proportions are determined by many factors (the annealing temperature, the duration of annealing, the pressing conditions, etc.).[162–166]

In the search for materials to be used in the manufacture of instruments and in construction, a study has been made of the Ti–C–B system.[157–166] An appreciable solubility of the diboride in TiC, an increased microhardness of the TiC_x-based phase, and some increase in the lattice parameter of the carbide have been noted for the TiB_2–TiC_x section.[157,158]

The conclusion reached initially[158] that the TiB and TiC_x components are infinitely miscible was not confirmed subsequently in the study of the section of the Ti–C–B phase diagram bounded by the TiB and TiC_x straight lines (x = 0.48–1.00). Three phases were identified in the specimens obtained: TiB_2, TiC_xB_4, and TiB (FeB structural type).

The phase formation process in the TiB–$TiC_{0.93}$ pseudobinary systems in the temperature range 1670–2070 K can be divided into two components according to X-ray diffractometric and scanning electron microscope data. Such subdivision is due to the different nature of the TiC_x interactions with the cubic and orthorhombic modifications of the monoboride.[165,166] The dominant involvement of the orthorhombic TiB in reactions leading to the formation of the higher borides Ti_3B_4 and TiB_2 has been postulated.

The quantum-chemical description of the heterophase systems is an extremely complex problem, which has not so far been solved. Only a few attempts[167–169] at calculations of the energy states of one of the components of the given polycrystalline materials—a borocarbide phase (a solid solution of the MC_xB_{1-x} type)—are known to have been made.

The local perturbation of the electron density of the hypothetical TiB following the introduction of a single carbon atom into the boron sublattice has been examined.[167] This simulated the initial stage in the formation of the $TiB_{1-x}C_x$ solid solution. The calculations were performed by the LMTO–GF method. The results indicate that the valence *s* and *p* functions of the carbon admixture are located in the region of the B 2*s* and Ti *d*,*s*–B 2*p* bands of the boride and the occurrence of the hybrid C–Ti–B interaction in the alloy cannot therefore be ruled out. Estimation of the perturbation of the LDOS of the titanium atoms (by the method described by Anisimov et al.[105]) shows, however, that the most marked effect, occurring when a boron atom is replaced by carbon, is the appearance of localised σ(Ti–C) bonds in the CTi_6 octahedron, as happens in refractory monocarbides.[103]

The converse problem, involving a single boron impurity atom at a C site of $TiC_{1.0}$, has been solved.[168] It is noted that the impurity states form two subbands. The lower subband has a markedly pseudoatomic form and corresponds to the localisation of the B 2*s* functions in the energy range between the C 2*s* and C 2*p*–Ti 3*d* bands. On the other hand, the B 2*p* states form a broad subband which overlaps almost fully the *p*–*d* hybrid band to TiC, indicating the formation of bonds of the Ti–B type in the TiC–B system.

A similar problem for the VC–B system has been solved by the LMTO-GF method.[169] Taking into account the uncertainty in the data concerning the processes involving the formation of the intergrain boundaries in the V–C–B system, the calculation was made for the case where boron substitutes both carbon and metal centres in $VC_{1.0}$. Whereas for the first type of substitution the LDOS of the impurity is similar to that for TiC–B, in the replacement of V by B (the formation of type

BC_6 'microclusters') the valence states of boron shift significantly into the region of lower bond energies, being partly superimposed on the C 2*s* states. Estimates of the change in the overall single-electron energy of the system show that ΔE in the latter is positive (~0.09 Ryd). This can be evidently attributed to the incomplete energy compensation for the 'rupture' of the strong V–C bonds due to the formation of new, weaker B–C bonds. Consequently, according to Sabiryanov,[169] in the solid-phase interaction of VC_x and boron (borides) the formation of borocarbides is less likely than that of vanadium borides.

A cluster analysis of the nature of the bonding in the Ti–C–B system has been carried out,[168] adopting titanium monocarbide as a basis. Its carbon sublattice was doped with boron atoms (the TiC_6Ti_{12}, TiC_5BTi_{12}, $TiC_4B_2Ti_{12}$, and $TiC_3B_3Ti_{12}$ fragments). The calculations were peformed in terms of the extended Hückel method (EHM). It was established that, when a carbon atom is replaced by a boron atom, the system of Ti–X (X = C, B) paired bonds is significantly transformed. Thus, if it is assumed that σ_{2p}(Ti–C) and π_{2p}(Ti–C) participate in the Ti–C interaction, then the Ti–B interaction includes the σ_{2s}(Ti–B), σ_{2p}(Ti–B), and π_{2p}(Ti–B) bonds, the populations of which (estimated in accordance with Mulliken's scheme) are comparable. In addition, the occurrence of a significant B–B interaction was established.

Hence, when account is taken of the known criteria of the formation of homogeneous solid solutions,[169–179] one may conclude that the absence of a continuous series of borocarbide solid solutions is associated with the specific features of the chemical bonds formed in the M–B–C systems apart from the dimensional factors.

Together with the variable-composition M–C–B solid solutions, fairly numerous crystalline *p* and *d* metal borocarbides have now been synthesised and their structures and some of their properties have been determined.[9,11] However, there have been no systematic studies of their microscopic properties and the available literature data refer solely to individual representatives of these compounds.

Table 6. The electron populations of bonds (e) in yttrium borocarbides.

Bond	YC_2	YBC	YB_2C_2	YB_2C	YB_4
Y–Y	0.351	0.165	0.235	0.302	0.121
Y–C	0.254	0.582	0.011	0.053	—
Y–B	—	0.196	0.372	0.400	0.827
C–C	1.785	0.012	1.236	0.012	—
C–B	—	1.339	0.976	1.321	—
B–B	—	1.457	1.245	2.132	2.736

A series of yttrium borocarbide phases, formed in the Y–B–C system and including the compounds YBC, YB_2C_2, and YB_2C, have been investigated[169] within the framework of the extended Hückel method. It was noted that there is a significant superposition of the (B, C) *s,p* and Y *s,p,d* states, the form of the LDOS of the individual centres depending critically on the type of their coordination in the crystal. This situation leads to the appearance of a complex system of interatomic bonds differing greatly in their nature and populations. The results presented in Table 6 show that, whereas the C–C interactions between pairs of nearest carbon atoms predominate in YC_2, in YBC there is competition between the B–B and C–B bonds, the role of the B–B bonds increasing with increase in the B/C ratio, which results in the formation of ordered structural motifs made up of the given atoms. It has been noted[169] that the B–B and B–C bonds arise as a consequence of the hybridisation of the B 2*s*,2*p*–C 2*p* orbitals, while the involvement of the metal atoms is secondary.

The Sc_2BC_2 alloy is yet another representative of borocarbides the electronic structure of which has been calculated within the framework of the extended Hückel and tight binding methods.[170] This phase (space group *I4/mmm*, lattice parameters $a = 3.300$ Å and $c = 10.691$ Å)[171] differs from most of the known lanthanide borocarbides, which have a layered structure,[172] by the fact that it contains in the bulk phase BC_2 groups similar to those present in the boron carbide $B_{13}C_2$.[173]

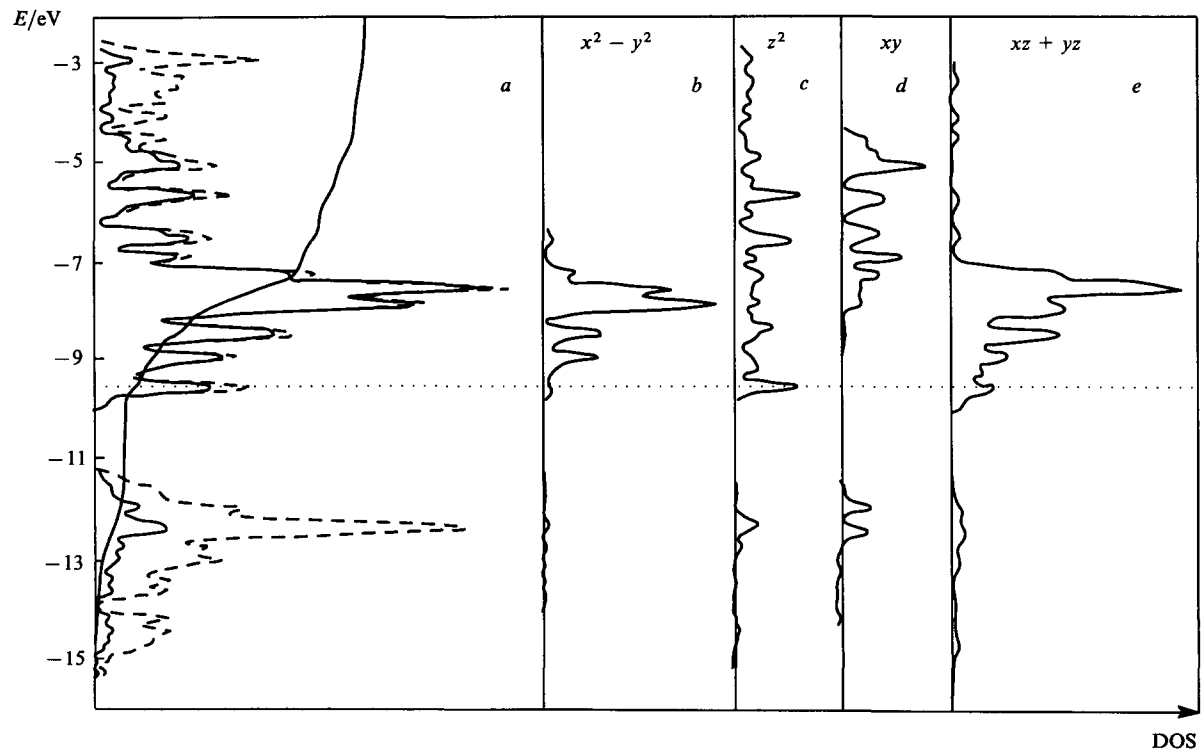


Figure 18. Densities of states in Sc_2BC_2:[170] (*a*) the total density of states of scandium (dashed curve) and the density of Sc 3*d* states (continuous curve); (*b*)–(*e*) partial contributions of the scandium *d* states.

EHM calculations for the BC_2 'molecule' indicate an appreciable separation of the nonbonding π_u- and antibonding π_u^* levels. The molecular charge has been estimated as approximately -5 e, i.e. this borocarbide can be regarded as a crystal containing the BC_2^{5-} anions. Allowance for the contribution by the atomic orbitals of the metal leads to a somewhat smaller overall charge (-2.48 e). The splitting of the electronic levels of the metal atom in the ligand field has been considered in relation to calculations for the $[ScB_5C_{10}]^{22-}$, $[Sc_2B_6C_{12}]^{25-}$, and $[Sc_2B_8C_{16}]^{35-}$ fragments with different configurations of the BC_2 groups.

The energy spectrum of Sc_2BC_2, obtained with the aid of the tight binding method, is presented in Fig. 18 (see previous page). Evidently, the low-energy bands are made up largely of the (B, C) 2*p* functions with an admixture of the Sc 3*d* orbitals and are separated from the nonbonding partly occupied bands by an energy gap. The Fermi level ($E_F \approx -9.5$ eV) is located in the region of the peak corresponding to the Sc 3*d* states, which is the reason for the metallic type of conductivity of the borocarbide.[171]

The energy dispersion of the bands in the pre-Fermi region suggests the anisotropy of the conductivity of Sc_2BC_2 when the Fermi level is intersected by the bands along the $\Sigma(M \rightarrow \Gamma)$ and $\Delta(\Gamma \rightarrow X)$ lines, which corresponds to the [010], [100], and [110] directions in the crystal. These bands are made up to the extent of 80%–100% of the Sc $d_{xz,yz,zz}$ states. Thus conduction is predominantly effected by Sc atoms separated by 3.144 Å distances in the (110) plane.

2. The M–B–N systems

As for the borocarbides, the available information about the phase relations in the M–B–N systems has remained extremely scattered and refers mainly to systems with participation of Group IVA and VA 3*d* and 4*d* metals. The efforts of investigators have been concentrated mainly on two aspects: on the creation of boronitride compositions of the TiB_2–TiN, ZrB_2–ZrN, and similar types[180–182] in order to improve the parameters of the initial phases and on the study of the formation of the boundary of the region of homogeneity in variable-composition boronitride phases.[183–187]

From the standpoint of the electronic theory, the description of the boronitride systems repeats that of borocarbide phases examined above and the difficulties arising are caused by the lack of correct methods permitting theoretical calculations for heterophase systems. The calculations of the energy states in the M–N–B systems carried out hitherto either involve the consideration of the problem of the single boron impurity in the nitride[167,168] or they resort to fragmentary approaches for the description of the transformation of the electronic states at the grain boundaries in composite boronitrides.[187,188]

In the first group of calculations, performed by LMTO-GF method for the TiN : B, ZrN : B, VN : B, and NbN : B impurity (as regards boron) systems, the form of the LDOS in boron was considered as a function of the EES of the matrix.[167,168] As in the case of the boron impurity in the carbides, the LDOS in the boron impurity in the nitrides has a two-peak structure comprising the B 2*s* and B 2*p* states, the degree of localisation of which (taking into account their position relative to the TiC and TiN valence bands) is found to be significantly more marked.

The rearrangement of the charge states and the system of orbital functions arising when a boron atom is incorporated in the cubic titanium nitride have been considered within the framework of the Mulliken–Wolfsberg–Helmholtz (MWH)[186,187] and X_α-DV [168] methods.

We may note that, according to the data of Zainulin et al.[185] the region of the existence of the homogeneous boronitride TiN_zB_y is extremely narrow: $z+y = 0.62-0.94$, $y \leqslant 0.03$. It follows from other data[186,187] that the electron energy spectrum of TiN_zB_y is markedly different from that of TiN. The lower group of orbitals, corresponding to the band of the quasi-core N 2*s* states, becomes narrower. The form of the rearrangement of the principal valence-bonding band is especially interesting. Whereas in TiN this band is made up predominantly of the N 2*p* states, which are significantly hybridised with metallic e_g-like orbitals, in TiN_zB_y an appreciable admixture of the B 2*s* states and a small admixture of B 2*p* states appears in TiN_zB_y in the region of the same energies. In the region of energies close to the edge of the filled part of the spectrum, there is an appreciable admixture of the 2*p* states of boron together with the Ti 3*d* type-t_{2g} atomic orbital.

Consequently, together with the Ti *d*–N 2*p* interaction, the Ti *d*–B 2*s* and Ti *d*–B 2*p* interactions play a significant role in TiN_zB_y. This becomes evident from an analysis of the bond populations and electronic configurations of the fragments for which calculations have been made.[186,187] The charge on the metal atom diminishes when boron atoms are introduced into its closest sphere. This finding is correlated with the results of a study[188] where the chemical shifts of the internal levels of the component atoms of a series of homogeneous TiN_xB_{1-x} solid solutions were investigated by electron microscopy.

Calculations have been made for simple octahedral clusters[186] in the Ti–N–B system for an increasing B/N ratio (the TiN_4B_2–TiN_2B_4 fragments). These groups can arise at the intergrain boundaries in polycrystalline boronitrides. It has been noted[186] that a steady increase in the number of states of the B *s,p* type entails a sharp alteration in the mechanism of interatomic bonding where Ti–B bonds of π_{2p} and σ_{2s} types predominate. Conversely, the Ti–N paired bonds are negligibly weak, which may affect the mutual diffusional mobility of the nitrogen and boron atoms and thus determine the processes involving the mutual dissolution of the boride and nitride phases.

3. The M–B–O system

A series of studies[167–169,187] have been devoted to the possibility of the partial substitution of oxygen atoms by boron atoms (in the TiO, VO, and ZrO structures) and to the formation of ternary solid solutions of the type MB_xO_{1-x}. Calculations for the VO : B system by the LCAO method have indicated, in particular, the appearance of a sharp anisotropy of the V–O and V–B bonds and also of significant B–B interactions, which may lead to the 'clustering' of the boron impurities in the bulk of the oxide.

Calculations by the LMTO method have been used[189] to predict the compositions of the possible stable cubic phases in the Ti–O–B system. The estimated energy of the substitution of B atoms by O atoms as well as the dependence of the total pressure and of the bonding and antibonding pressures on the number of valence electrons (in the range 6.5–9 e) indicate the probable existence of the stable phase $TiB_{0.75}O_{0.25}$.

A series of phases of the M–B–O systems with individual structural types have been examined.[190,191] The electronic spectrum of $Li_2B_4O_7$—a promising material for acousto-electronics—has been calculated.[190] Taking into account the characteristic features of the crystal structure of $Li_2B_4O_7$ [192] and on the basis of phonon spectra,[193] a series of structural fragments (BO_3, BO_4, LiO_4, LiO_6) were identified in the crystal and for each of them a secular equation was set up. The effect of environment was taken into account within the framework of the perturbation theory. The interband intervals were corrected on the basis of the maxima in the imaginary component of the relative permittivity.

The band structure of $Li_2B_4O_7$ thus obtained represents in essence a superposition of the electronic states of the structure-forming elements of the phase, included in the consideration and arranged in an energy sequence.[190] It was noted that the covalent bonds in the boron–oxygen groups are the most significant (degree of covalence ~ 0.94, Harrison's data[194]), but the maximum mount of ionic character (~ 0.17) was found in the LiO_{4-6} fragment.

Problems concerning the chemical bonding in $LiBO_2$, which is formed in the Li–B–O system, have been examined[191] with the aid of the X-ray diffraction method and dynamic deformation electron density (DED) maps.[195–197] The crystal structure of

$LiBO_2$ can be represented as an assembly of BO_3 'triangles' making up the chain and oriented in the $(\bar{1}05)$ plane, the lithium atoms being located in their vicinity.[198] There are different B–O distances in the BO_3 groups, varying in the range from 1.324 to 1.409 Å. The differences in the distance from the lithium atom to the oxygen atoms constituting its closest sphere (1.955–2.473 Å) are extremely significant.

The published[191] DED maps indicate the formation of B–O covalent bonds in the BO_3 groups. The estimated amount of ionic character of the bonding indicates the B → O charge transfer. The charges are (assuming +1 for Li) 2.6+ for B, 1.8– for O^1, and 1.9– for O^2. The DED maps for planes incorporating lithium demonstrate only a slight overlap of the cationic and oxygen states. The interaction of lithium with its environment in the metaboride is therefore largely electrostatic.

4. The M–B–P systems

The preparation of the crystalline borophosphide $Fe_3(P_xB_{1-x})$ has been reported.[199] The initial interpretation of its properties was based on a simplified model postulating charge transfer from nonmetal atoms to the iron atom.[200,201]

The ternary $Fe_3B_{0.9}P_{0.1}$ alloy (Fe_3B structural type) has been investigated[202] by photoelectron X-ray spectroscopy (AlK_α radiation, ~0.2 eV resolution) with the aid of the method described by Wertheim and coworkers.[203,204] The binding energies for the Fe 3*s*,3*p*, P 2*p*, and B 1*s* core levels were determined and were found to be similar to those for the pure elements (within the limits of experimental error), which precludes the hypothesis of an ionic model for the given alloy. The X-ray photoelectron spectra of Fe, Fe_3P, and $Fe_3B_{0.9}P_{0.1}$ demonstrate a fairly complex profile of the spectral lines.[202] Taking into account the degrees of photoionisation of states of different symmetry, one may claim that the most intense pre-Fermi maxima correspond to emission from the band of *d* states. The lower energy maxima correspond to states similar to B *s*,*p*. The widths of the valence bands, which are ~17 eV for Fe_3P and ~14 eV for $Fe_3B_{0.9}P_{0.1}$, differ appreciably.

On the basis of calculations,[201] the high-energy maxima were assigned to the *s* states of iron and nonmetals, while the lower-energy peaks reflect the splitting of the *d* functions of the iron atoms in structurally nonequivalent positions and their mixing with the *p*-type subbands of phosphorus and boron. Finally, the greater width of the spectrum at the half maximum level in the case of $Fe_3B_{0.9}P_{0.1}$ (5.1 eV) compared with Fe_3P (4.5 eV) is treated as a consequence of the shorter Fe–B distances and greater hybridisation of their valence orbitals. Hence it follows that the observed change in the magnetic moments and parameters of the hyperfine fields on formation of the ternary iron alloys is associated with the reordering of the orbitals of the iron atoms as a result of interactions with the atoms in the immediate environment and not with electron transfer effects.[198]

V. Metal–metal–boron ternary systems

All the ternary compounds formed in metal–metal–boron systems can be arbitrarily divided into two groups.[11] The first comprises ternary boride phases having individual crystal structures, while the second consists of solid solutions with limited or infinite miscibility on formation of which the substitution of part of the metal atoms of the binary phase by metal atoms of a different kind takes place statistically.

Most of the studies on the electron energy spectra of ternary ordered phases by quantum-chemical methods have been devoted to compounds containing *f* elements. Their consideration is outside the scope of the present review. We shall only mention studies[205–207] in which band calculations were performed for the borides $Y_2Fe_{14}B$ and $Y_2Co_{14}B$. By virtue of their magnetic characteristics, the latter have attracted attention as promising materials for the construction of permanent magnets.[208,209]

Calculations by the LCAO method[205] and in terms of the tight binding model,[206,207] carried out for the above borides, lead to similar electron energy spectra of these compounds: the valence band is made up predominantly of a complex superposition of Fe(Co) states which are significantly different for structurally

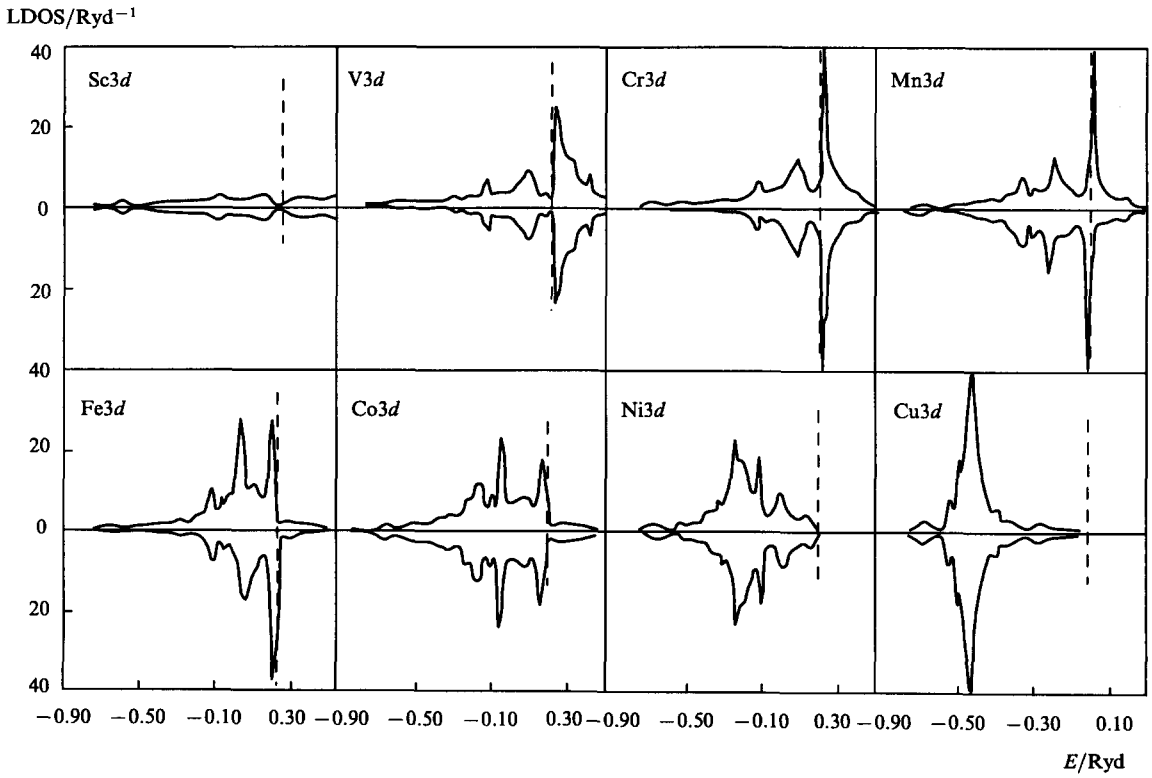


Figure 19. The local densities of states of 3*d* impurities in TiB_2. Spin-polarised calculation by the LMTO-GF method.

nonequivalent centres (six positions) with an admixture of yttrium and boron states. Most attention has been devoted in the above investigations [205-207] to calculations of the magnetic parameters of the phases. It was established that, depending on the type of the immediate environment, the local magnetic moments (LMM) on the iron atoms in $Y_2Fe_{14}B$ can vary appreciably (from 2.11 to 2.74 μ_B); the local magnetism for $Y_2Co_{14}B$ is appreciably weaker — the LMM on the cobalt atoms vary in the range 1.28 to 1.48 μ_B.

The energy states of the 3*d* metal impurities in TiB_2 (these systems can be treated as the starting materials in the formation of $M_xTi_yB_2$ solid solutions) have been investigated [210] by the LMTO-GF method. The local densities of states of the impurity elements make it possible to trace the rules governing their formation throughout the series of 3*d* metals (Fig. 19).

Evidently, the similarity of the orbital energies of the dopand metal atoms at the beginning of the *d* series (Sc, V) to the energies of the states of the titanium atom promotes the establishment of a LDOS similar to that for titanium. The LDOS for the *d* metals at the end of the series assume a significantly different form. With increase in the valence of the impurity (on passing from Cr to Cu), there is a progressive low-energy shift of the occupied states of the dopand atoms with generation of additional (nonbonding) DOS lines in the region of a local minimum in the spectrum of the matrix (between the *s*- and *p*-like bands) and also in the vicinity of the lower edge of the valence band of the diboride. This effect can be traced most distinctly for the LDOS in copper.

The increase in the concentration of the impurity states in the region of the principal bonding bands of TiB_2 indicates an increase in the covalent component of the bonding in the ternary systems. The estimated changes in the total one-electron energy of the matrix following the introduction of the dopands (ΔE) are presented in Fig. 20. Although in terms of the single-site approximation these quantities can reflect only the qualitative behaviour in the series of such systems, we may note that the substitution of Ti atoms by Sc and V atoms leads (as for the *d* metals at the end of the series) to the destabilisation of the system of interatomic bonds in the crystal. Conversely, it follows from the data obtained that doping of the diborides with admixtures of Cr, Mn, Fe, and Co tends to decrease the one-electron energy. This can indicate stronger binding of the additives in the bulk of TiB_2 compared with the centre being substituted.

The transformation of the high-energy *d* band of the impurity (which is unoccupied for Sc and V) is of interest. With increase in the atomic number of the impurity element, the energy of the *d* band falls sharply and, for example, in the case of chromium, is located in the immediate vicinity of E_F, being subsequently partly (Mn, Fe) or completely (Co, Cu) filled. Such behaviour of the LDOS leads to the appearance of spin polarisation with splitting of the bands corresponding to the opposite spin orientation and hence the formation of appreciable LMM on centres comprising *d* metals in the middle of the series (Fig. 20). This finding can be accounted for on the basis of Stoner's criteria, according to which one of the conditions for the formation of the LMM in the crystal is a high DOS in the vicinity of E_F, which is in fact observed for chromium, manganese, and iron. For cobalt, nickel, and copper, these states are fully occupied and there are therefore no magnetic moments on the given atoms.

In conclusion, we may note that the results agree with those obtained for the series of 3*d* and 4*d* metal carbides and nitrides. This suggests that the characteristics of the band structure of the matrix, in the first place the presence of a deep DOS minimum in the vicinity of the Fermi level, are decisive in the generation of local magnetic moments on *d* impurities in binary phases. One may expect that a similar situation occurs also in the ZrB_2: M and HfB_2: M systems (M = 3*d* metal), while the 4*d* impurities in diborides are nonmagnetic in the vast majority of cases.

VI. Amorphous metal borides

We shall consider yet another class of boron-containing systems — amorphous metal borides [metallic glasses (MG)], which exhibit interesting mechanical properties, a high corrosion resistance, and a series of unusual magnetic characteristics. [210,211]

There are several phenomenological theories which explain the stability of the amorphous state of the glasses near the composition $M_{80}X_{20}$. In the model proposed by Nagel and Tauc, [212] the metallic glasses are described as systems with almost free electrons. Their stability is explained by the position of the Fermi level in a deep DOS minimum, which is attained by introducing nonmetal atoms into the alloy. The role of such atoms reduces to the regulation of the electron concentration in the system. In the statistical theory taking into account the degree of packing of 'hard spheres' (metal atoms), the involvement of *p* elements is accounted for by the need to fill the cavities in the polyhedra of the 'matrix'. This is manifested most effectively for the ratio $M/X \approx 4$. [213] The possible role of chemical metal–nonmetal bonding in the transition of the system to the amorphous state has been pointed out by Shen and Park. [214]

The role of chemical bonding has been analysed within the framework of fragment models. [215,216] A calculation has been carried out [215] for the $[Ni_2Fe_2B]$ group in the $Ni_{40}Fe_{40}B_{20}$ structure by the spin-polarised multiple scattering method (Fig. 21). The structure is represented with the aid of Bernal polyhedra, the

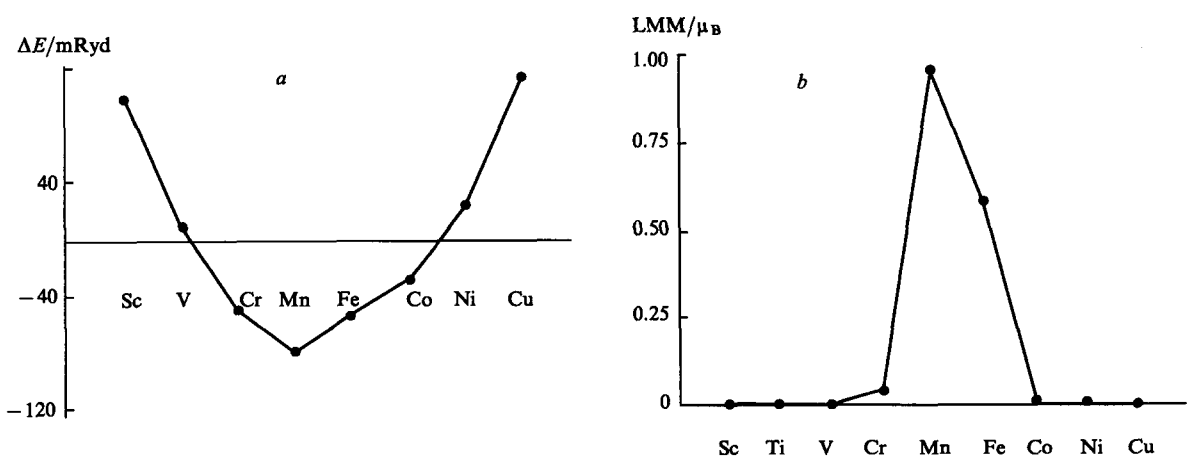


Figure 20. The changes in the total one-electron energy of TiB_2 on introduction of *d* metal impurities (*a*) and in the local magnetic moment on the 3*d* centres in TiB_2 (*b*).

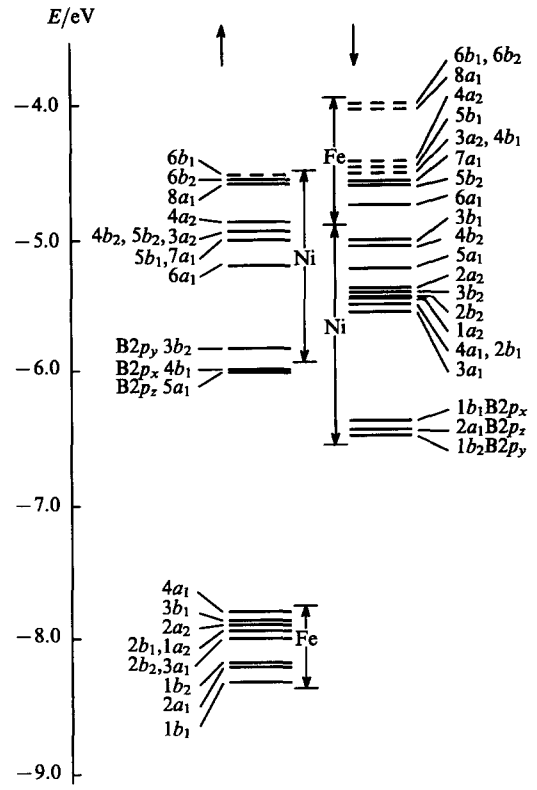


Figure 21. Molecular orbital diagram for the Ni_2Fe_2B cluster. Spin-polarised calculation by the scattered wave method.

smallest cluster (a tetrahedron) simulating the alloy being employed. A significant hybridisation of the boron *p* states with a series of low-energy molecular orbitals containing an appreciable contribution due to Ni *d* orbitals has been established. The boron–iron states exhibit a much smaller overlap. The local nature of these bonds and their anisotropy have been emphasised.[215] In this case, the charge density is concentrated mainly in the BNi_2 plane, which indicates the preferential bonding of boron to one of the metals, namely nickel. This results in the formation of microclusters of the type BNi_x in the metallic glass region.[217]

A similar approach has been used in calculations for the $[Co_8B_2]$, $[Co_4Fe_4B_4]$, $[Co_8B_4]$, and $[Fe_8B_4]$ clusters taking into account the possible formation of direct B–B bonds.[216] The greater stability of the $[Co_8B_2]$ system, compared with $[Co_8]$, has been interpreted[217] as a consequence of the decrease in the energy of a series of molecular orbitals (by ~1 eV) genetically related to the Co 3*d* states. This is due to their mixing with the B 2*p* functions accompanied by a weakening of the Co–Co bonds. The introduction of the iron impurity into the alloy hardly affects the energy states of cobalt, i.e. the decisive role of the Co–B bonds is retained, which leads to the appearance of local Co_nB ordering in the bulk of the metallic glass. It has been concluded[217] that cluster type boride metallic glasses (Co_3B, Fe_3B) are more stable than the corresponding crystal structures.

An attempt has been made to apply to the description of the amorphous $Fe_{80}B_{20}$ alloy the spin polarised LMTO method developed for calculations relating to invariant crystals.[218] A structure of the Fe_4N type, in which the coordination numbers of the Fe and N atoms are closest to those in the amorphous alloy, was selected as a model.[219–221] It was established that the conductivity band of the 'Fe_4B' metallic glass is determined by the states of the iron atom while the Fe 3*d*–B 2*p* hybridised states are concentrated near the bottom of the conductivity band (Fig. 22).

A fairly extensive series of studies have been carried out in recent years on the modification of the band approaches to calculations on amorphous systems.[222–231] Thus the problem of the relation between atomic structure and electron distributions in the $Fe_{100-x}B_x$ amorphous alloys has been considered.[222] The structure of the metallic glass was described in terms of an assembly of particles (several hundreds) interacting in accordance with the Morse function. The densities of states were calculated by the recursion method for a tight binding Hamiltonian with Harrison's parametrisation. A satisfactory agreement was obtained between the calculated data and experimental atomic radial distribution functions. The agreement between theoretical electronic and photoemission data is satisfactory.

The magnetic properties of $Fe_{100-x}B_x$ valence bonds amorphous alloys have been calculated.[230] Using the spin-polarised LMTO tight binding method and the recursion technique, the hyperfine fields on the iron nuclei as well as the isomeric shifts were calculated. The results agree quite well with Mössbauer spectroscopic data. A correlation was established between the directions of the shifts and the local environment of the ^{57}Fe nuclei (the number of boron atoms in the first coordination sphere of iron).

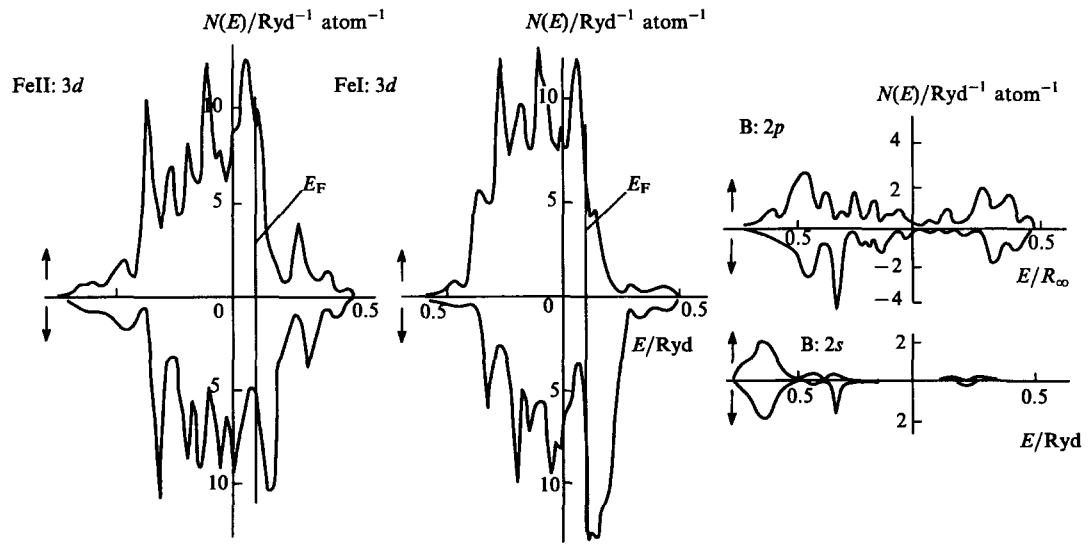


Figure 22. Partial densities of states in Fe_4B. The designations FeII and FeI correspond to iron atoms in the first and second coordination spheres of boron.

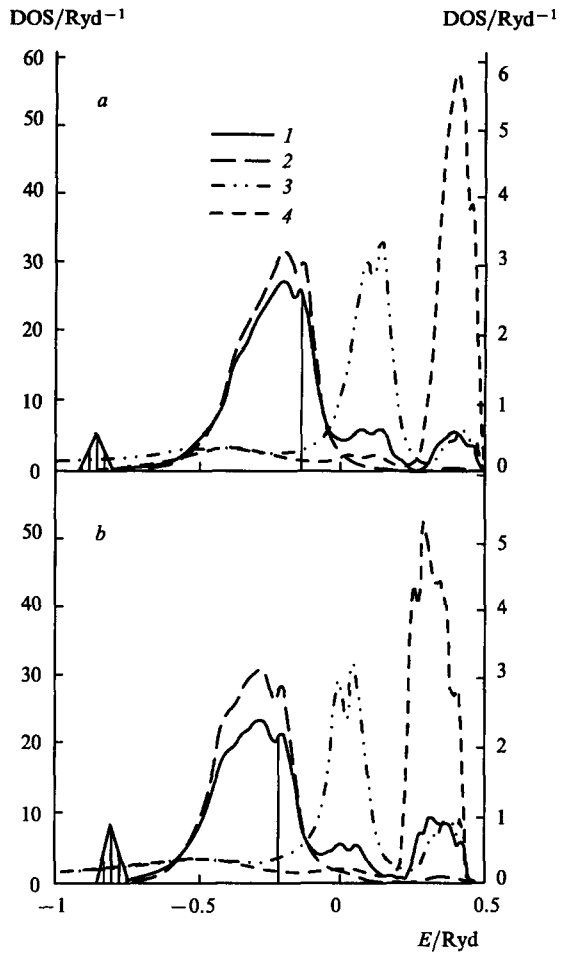


Figure 23. The total density of states (curve *1*) and the partial densities of Fe 3*d* (curve *2*), Fe 4s (curve *3*), and B 2*p* (curve *4*) states in the $Fe_{85}B_{15}$ (*a*) and $Fe_{75}B_{25}$ (*b*) amorphous alloys. The cross-hatched triangles indicate the position and 'centre of gravity' of the B 2*s* bands.

The structures of the $Fe_{85}B_{15}$ and $Fe_{75}B_{25}$ valence bands (Fig. 23) have been calculated by the LMTO method in terms of the atomic spheres approximation (LMTO ASA) and the recur-sion method.[228] The valence band of the alloy is made up of hybridised Fe 3*d*–B 2*p* states, the contributions of which to the occupied part of the spectrum vary in accordance with the composition of the boride. With increase in the boron content, the local magnetic moment diminishes from 1.795 μ_B for $Fe_{85}B_{15}$ to 1.705 μ_B for $Fe_{75}B_{25}$. The relation between the electronic parameters and the atomic configurations of the metallic glass has also been discussed in other investigations.[224–226]

The LMTO ASA method combined with the recursion technique has been used in calculations for a metallic glass of the $Co_{100-x}B_x$ (x = 17, 23, and 32) type.[231] As in the case of $Fe_{100-x}B_x$, the valence band of cobalt boride is of the Co 3*d*–B 2*p* hybrid type and the bonds between unlike atoms are determined by the Co–B covalent interactions. The charge transfer from Co to B is insignificant (~0.68 e) and is stable for the concentrations considered. The local magnetic moment diminishes sharply as the alloy becomes enriched in boron (for example, from 1.32 μ_B for $Co_{83}B_{17}$ to 0.94 μ_B for $Co_{68}B_{32}$).

Whereas the range of metallic glasses for which theoretical calculations have been made is fairly limited, the class of such glasses whose electronic structure has been investigated experimentally is much more extensive:

Alloy	Ref.
$Fe_{80}B_{20}$	234, 243, 247
Fe_xB_{100-x} (x = 88, 87, 86, 80, 75)	239, 255
$Fe_{1-x}B_x$ ($x \leqslant 0.2$)	246
Fe_xB_{100-x} (x = 86, 82, 28, 24, 20)	248
$Co_{80}B_{20}$	232
$Fe_{82}B_{18}$; $Ni_{81.5}B_{18.5}$	253
$Co_{81.5}B_{18.5}$	248
$Co_{76}Fe_4B_{20}$; $Co_{70}Fe_{10}B_{20}$	233
$Co_{80-x}Fe_xB_{20}$ (x = 6, 10, 20)	232
$Co_{85-x}Fe_xB_{15}$ (x = 65, 73)	235
$Fe_{80}M_3B_{17}$ (M = Fe, Co, W, Pt)	235
$Fe_{40}Ni_{40}B_{20}$	234, 243
$Fe_{75}Si_{10}B_{15}$; $Ni_{75}Si_{10}B_{15}$	253
$Fe_{76}Si_{12}B_{12}$; $Fe_{76}Si_{18}B_{12}$	248
$FeSi_{10}B_{12}$; $Fe_{45}Ni_{45}P_{8.5}B_{1.5}$	244
$Fe_{40}Ni_{40}P_{14}B_6$; $Fe_{32}Ni_{36}Cr_{14}P_{12}B_6$	252
$Fe_{82}B_{18-x}Be_x$	254
$Ni_{40}Fe_{40}P_{14}B_6$	251
$Fe_{70}Ni_8Si_{10}B_{12}$	250
$Co_{78}P_{14}B_8$	249
$Fe_{40}Ni_{40}P_{16}B_6$	234, 242, 245
$Fe_{67}Co_{18}B_{14}Si_{12}$	236
$Fe_{40}Ni_{38}Mo_4B_{18}$; $Ni_{76}Si_{12}B_{12}$	237
$Fe_{32}Ni_{32}Cr_{14}P_{12}B_6$	238
$Ni_{36}Fe_{32}Cr_{14}P_{12}B_6$	240, 241

The main problem discussed in the above investigations involves the consideration of the energy structure of the amorphous alloys, the establishment of the differences between the electron energy spectra of the amorphous and crystalline states, and also the determination of relations of the composition–property type for a fairly representative set of systems.

The BK_α-XES presented as an example in Fig. 24 for a series of metallic classes and crystalline phases based on iron and nickel and their joint representation in terms of a single energy scale with K_β and L_α lines[253] illustrate the main results obtained within the framework of the approaches mentioned above. Thus the following points have been noted:[253] (1) the valence band of the metallic

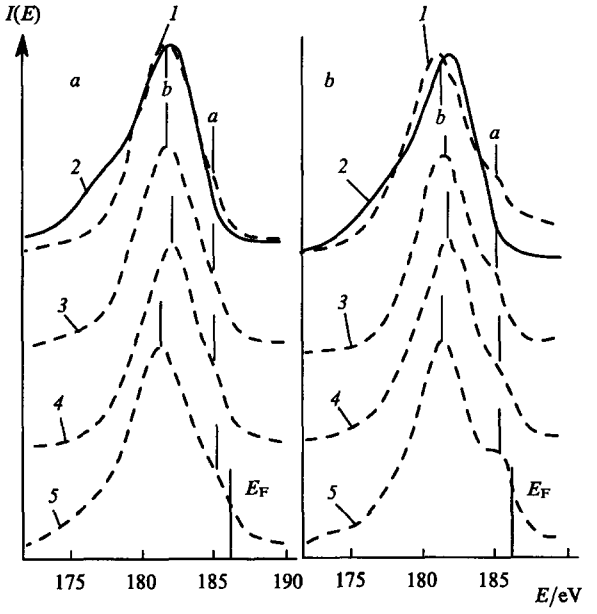


Figure 24. The BK_α X-ray emission spectra of amorphous iron and nickel borides and the spectrum of crystalline boron. (*a*): (*1*) α-$Fe_{82}B_{18}$; (*2*) B (crystalline); (*3*) α-$Fe_{75}Si_{10}B_{15}$; (*4*) Fe_2B; (*5*)FeB; (*b*): (*1*) α-$Ni_{81.5}B_{18.5}$; (*2*) B (crystalline); (*3*) α-$Ni_{75}Si_{10}B_{15}$; (*4*) Ni_2B; (*5*) NiB.

glass is made up of overlapping subbands of the B $2p$–(Fe, Ni) $3d$ states; (2) the maximum in the BK_α spectrum (peak *b*) is located near the bottom of the valence band and the substructure *a* [the intensity of which diminishes with increase in the (Fe, Ni)/B ratio], can be clearly traced on the short-wavelength slope of the line; (3) apart from the main maximum (located in the pre-Fermi region, which indicates the predominance of states with $3d$ symmetry near E_F), bulges, which have the same energies as the *a* and *b* maxima of the BK_α line, can be clearly seen in the L_α spectra, indicating an appreciable hybridisation of the B $2p$–(Fe, Ni) $3d$ states; (4) the peaks in the BK_α spectra of nickel-based metallic glasses, corresponding to the bonding states of NiB, are the most intense and are displaced into the long-wavelength part of the spectrum relative to the Fe-containing metallic glasses (this is probably the reason why Ni–B interactions are preferred in more complex systems containing simultaneously the Fe and Ni components); (5) comparison of the characteristics of the XES of the metallic glasses [similar to those noted in (4)] with those of binary crystals may indicate the probable cause of the transition to the amorphous state and its stability.

The XES, ES, and ESCA methods have also been used to investigate the chemical shifts of the inner levels (charge states) in metallic glasses,[233,235,238,239,252] for the description of the effects of the doping of the metallic and nonmetallic 'sublattices' of the glasses,[232,235,238,240–242,244,245,250,255] and for the oxidation of surfaces of amorphous materials.[238,250] The optical properties of boride metallic glasses have been considered, for example, by Lustig et al.[246]

In conclusion, we may note a series of studies[234,236,241] in which transitions from the crystalline to the amorphous state in a series of binary iron, cobalt, and nickel alloys and the compositions of the surfaces of the latter were investigated by Auger electron spectroscopy. In particular, the concentration profiles constructed for the distribution of the elements in the 'bulk' of $Fe_{80}B_{20}$ and $Fe_{40}Ni_{40}P_{16}B_4$ specimens[234] indicate the enrichment of their surface layers in the nonmetals during crystallisation.

This review has been written with the financial support of the Russian Fundamental Research Fund (Project No. 94-03-09524).

References

1. G V Samsonov, L Ya Markovskii, A F Zhigach, M G Valyashko *Bor, Ego Soedineniya i Splavy* (Boron, Its Compounds and Alloys) (Kiev: Izd. Akad. Nauk Ukr. SSR, 1960)
2. G V Samsonov, Yu B Paderno *Boridy Redkozemel'nykh Metallov* (Borides of Rare-earth Metals) (Kiev: Nauk. Dumka, 1961)
3. B Post, F W Glaser *Refractory Binary Borides* (New York: Interscience, 1963)
4. T Lundstorm, S Rundqvist *Borides, Silicides and Phosphides* (London: Methuen, 1965)
5. W G Wyckoff *Crystal Structures* Vol. 1 (New York: Wiley, 1963)
6. B Post *Refractory Binary Borides, Metallo-Boron Compounds and Boranes* (New York: Wiley, 1964)
7. E L Muetterties *The Chemistry of Boron and Its Compounds* (New York: Wiley, 1967)
8. R Thompson *Prog. Boron Chem.* **2** 173 (1970)
9. J Goldschmidt *Interstitial Phases* (Translated into Russian; Moscow: Mir, 1971)
10. G V Samsonov, T I Serebryakova, V A Neronov *Boridy* (Borides) (Moscow: Atomizdat, 1975)
11. Yu B Kuz'ma *Kristallokhimiya Boridov* (Crystal Chemistry of Borides) (Lvov: Vishcha Shkola, 1983)
12. T Ya Kosolapova (Ed.) *Svoistva, Poluchenie i Primenenie Tugoplavkikh Soedinenii: Spravochnik* (Properties, Preparation and Applications of Refractory Compounds: Handbook) (Moscow: Metallurgiya, 1986)
13. T Lindstrom *Pure Appl. Chem.* **57** 1383 (1985)
14. *Boridy i Materialy na Ikh Osnove. Sbornik Trudov* (Borides and Materials Based upon Them. Collected Works) (Kiev: Nauk. Dumka, 1986)
15. G V Samsonov, G Sh Upadkhaya, V S Neshpor *Fizicheskoe Materialovedenie Karbidov* (Physical Materials Technology of Carbides) (Kiev: Nauk. Dumka, 1974)
16. G V Samsonov, I M Vinitskii *Tugoplavkie Soedineniya* (Refractory Compounds) (Moscow: Metallurgiya, 1976)
17. G V Samsonov, I F Pryadko, L F Pryadko *Elektronnaya Lokalizatsiya v Tverdom Tele* (Localisation of Electrons in Solids) (Moscow: Nauka, 1976)
18. Yu M Goryachev, B A Kovenskaya, G V Samsonov *Izv. Vyssh. Uchebn. Zaved. Fiz.* **8** 86 (1974)
19. W N Lipscomb, D Britton *J. Chem. Phys.* **33** 275 (1960)
20. E Dempsey *Philos. Mag.* **8** 285 (1983)
21. G V Samsonov, Y M Goryachev, B A Kovenskaya *J. Less-Common Met.* **47** 147 (1976)
22. K E Spear *J. Less-Common Met.* **47** 123 (1976)
23. J Piper *J. Phys. Chem. Solids* **27** 1907 (1966)
24. R Kiessling *Fortschr. Chem. Forsch.* **3** 41 (1954)
25. S T Serebryakova *J. Less-Common Met.* **67** 499 (1979)
26. P G Perkins, A V J Sweeney *J. Less-Common Met.* **47** 165 (1976)
27. H S Lonquet-Higgins, M V Roberts *Proc. R. Soc. London, Ser. A* **224** 336 (1954)
28. A L Ivanovskii, I V Shein *Izv. Akad. Nauk SSSR, Neorg. Mater.* **27** 2103 (1991)
29. M Yamazaki *J. Phys. Soc. Jpn.* **12** 1 (1957)
30. S Flodmark *Ark. Fys.* **18** 49 (1960)
31. S Flodmark *Ark. Fys.* **14** 513 (1959)
32. S Flodmark *Ark. Fys.* **9** 1357 (1955)
33. W N Lipscomb, D Britton *J. Chem. Phys.* **33** 275 (1960)
34. Yu B Paderno, Yu M Goryachev, E S Graf, in *Redkozemel'nye Metally i Ikh Soedineniya* (Rare-earth Metals and Their Compounds) (Kiev: Nauk Dumka, 1970) p. 101
35. P G Perkins, D R Armstrong, A Breeze *J. Phys. C, Solid State Phys.* **8** 3558 (1975)
36. R W Johnson, A H Daane *J. Phys. Chem.* **65** 909 (1961)
37. H Ichara *Res. Electrotech. Lab.* **125** 775 (1977)
38. A Hasegawa, A Yanase *J. Phys. C, Solid State* **12** 5431 (1979)
39. D D Koelling, B N Harman *J. Phys. C, Solid State Phys.* **10** 3107 (1977)
40. M Aono, S Kawai, S Kono *J. Phys. Chem. Solids* **37** 215 (1976)
41. I I Lyakhovskaya, T M Zimkina, V A Fomichev *Fiz. Tverd. Tela* **12** 174 (1970)
42. L Ramqvist, B Ekstig, E Kallne, E Noreland, R Manne *J. Phys. Chem. Solids* **30** 1849 (1969)
43. D W Fisher, W L Baum *J. Appl. Phys.* **39** 4757 (1968)
44. V G Aleshin, T Ya Kosolapova, V V Nemoshkalenko, T I Serebryakova, N G Chudinov *J. Less-Common Met.* **67** 173 (1979)
45. V G Alyoshin, T I Serebryakova, A I Kharlamov *Phys. Status Solidi B* **83** 537 (1977)
46. I I Lyakhovskaya, T M Zimkina, V A Fomichev *Izv. Akad. Nauk SSSR, Ser. Fiz.* **36** 393 (1972)
47. E Z Kurmaev, S A Nemnonov, V P Belash, Yu V Efimov *Fiz. Met. Metalloved.* **33** 578 (1972)
48. J Wong, F W Lytle, R P Messmer, D H Maylotte *Phys. Rev. B, Condens. Matter* **30** 5596 (1984)
49. E A Zhurakovskii, V P Dzeganovskii, T N Bondarenko *Metallofizika* **7** 37 (1971)
50. E A Zhurakovskii, V P Dzeganovskii, T N Bondarenko *Ukr. Fiz. Zh. (Russ. Ed.)* **15** 1477 (1970)
51. I N Frantsevich, E A Zhurakovskii, N N Vasilenko *Ukr. Fiz. Zh. (Russ. Ed.)* **14** 1065 (1970)
52. S I Salem, C N Chang, T J Nash *Phys. Rev. B, Solid State* **18** 5168 (1978)
53. C Senenaud, C Hagne *J. Phys. (Paris)* **4** 193 (1971)
54. T B Shashkina, B I Kotlyar, E A Zhurakovskii *Teor. Eksp. Khim.* **7** 686 (1971)
55. E A Zhurakovskii *Dokl. Akad. Nauk Ukr. SSR, Ser. B* **3** 240 (1967)
56. R B Singh, S K Händel, B Stenerhag *Z. Phys.* **249** 241 (1972)
57. T B Shashkina, B I Kotlyar, E A Zhurakovskii *Izv. Vyssh. Uchebn. Zaved. Fiz.* **6** 16 (1970)
58. V V Nemoshkalenko, A I Kharlamov, T I Serebryakova, V G Aleshin *Kinet. Katal.* **19** 1567 (1978)
59. A V Koval', S M Karal'nik *Izv. Vyssh. Uchebn. Zaved. Fiz.* **8** 17 (1978)

60. S Falch, G Rainer-Harbach, F Schmuckle, S Steeb *Z. Naturforsch. A* **36** 937 (1981)
61. D J Joyner, O Johnson, D M Hercules *J. Am. Chem. Soc.* **102** 1910 (1980)
62. O Johnson, D J Joyner, D M Hercules *J. Phys. Chem.* **84** 542 (1980)
63. D J Joyner, O Johnson, D M Hercules *J. Phys. F, Met. Phys.* **10** 169 (1980)
64. V G Alyoshin, A I Kharlamov, V M Prokopenko *J. Solid State Chem.* **38** 105 (1981)
65. G Mavel, J Escard, P Costa, J Castaing *Surf. Sci.* **35** 109 (1973)
66. D J Joyner, R F Willis *Philos. Mag.* **43A** 815 (1981)
67. M P Arbuzov, B I Kotlyar, T B Shashkina, et al. *Izv. Vyssh. Uchebn. Zaved. Fiz.* **6** 52 (1972)
68. D J Joyner, O Johnson, D M Hercules, D W Bullett, J H Weaver *Phys. Rev. B, Condens. Matter* **24** 3122 (1981)
69. A Amamon, G Krill *Solid State Commun.* **31** 971 (1979)
70. E A Zhurakovskii, T B Shashkina, B I Kotlyar *Izv. Vyssh. Uchebn. Zaved., Fiz.* **1** 24 (1970)
71. K Tanaka, T Saito, K Suzuki, R Hasegawa *Phys. Rev. B, Solid State* **32** 6853 (1985)
72. M I Korsunskii, Ya E Genkin *Izv. Akad. Nauk Kaz. SSR, Ser. Fiz.-Mat.* **2** 77 (1967)
73. M I Korsunskii, Ya E Genkin, V G Lifshits *Izv. Akad. Nauk Kaz. SSR, Ser. Fiz.-Mat.* **4** 62 (1975)
74. E V Petrov, V V Tsvetkov *Metallofizika* **40** 98 (1972)
75. P H Middleton, A J Paul, P M A Sherwood *J. Chem. Soc., Faraday Trans. 1* **80** 2549 (1984)
76. E V Petrov *Metallofizika* **44** 83 (1973)
77. Yu M Shul'ga, S Yu Zasedatelev, Yu G Borodko, E A Blyumberg *Metallofizika* **44** 787 (1973)
78. E A Zhurakovskii, A A Vladimirova, V P Dzeganovskii *Dokl. Akad. Nauk SSSR* **170** 548 (1966)
79. D R Wheeler, W A Brainard *J. Vac. Sci. Technol.* **15** 24 (1978)
80. E A Zhurakovskii, V V Gorskii *Dokl. Akad. Nauk Ukr. SSR* **11** 1428 (1966)
81. E A Zhurakovskii, V I Kotlyar, T B Shashkina *Dokl. Akad. Nauk Ukr. SSR* **7** 654 (1969)
82. T B Shashkina *Phys. Status Solidi B* **44** 571 (1971)
83. E S Konovalova, Yu V Paderno, in *Vanadaty i Boridy RZM. Sintez i Svoistva* (Vanadates and Borides of Rare-earth Metals. Synthesis and Properties) (Sverdlovsk: Ural'sk. Nauch. Tsentr Akad. Nauk USSR, 1982) p. 28
84. K Spear *Refract. Mater.* **6** 91 (1976)
85. S Gajima, K Niihara, in *Abstracts of Reports at the IXth RE Research Conference, Blackburg, Virginia, 1971* p. 23
86. W Hoffmann, W Janiche *Z. Metallkd.* **28B** 1 (1936)
87. V A Neronov *Zh. Neorg. Khim.* **14** 1704 (1969)
88. V T Serebryanskii, V A Epel'baum, G S Zhdanov *Zh. Neorg. Khim.* **12** 2486 (1967)
89. V T Serebryanskii, V A Epel'baum, G S Zhdanov *Dokl. Akad. Nauk SSSR* **141** 885 (1967)
90. G Will *Nature (London)* **212** 175 (1966)
91. G Will *J. Am. Chem. Soc.* **85** 2335 (1963)
92. G Will *Acta Crystallogr.* **23** 1071 (1967)
93. V N Gurin, M M Korsukova, in *Boron and Refractory Borides* (Berlin: Springer, 1977) p. 293
94. R Greatrex *Annu. Rep. Prog. Chem., Sect. A* **81** 29 (1984)
95. J A Kohn, A A Giardini *Z. Kristallogr.* **111** 53 (1958)
96. J K Burdett, E Canadell, G J Miller *J. Am. Chem. Soc.* **108** 6561 (1986)
97. D R Armstrong, A Breeze, P G Perkins *J. Chem. Soc., Faraday Trans. 2* **7** 952 (1977)
98. I I Lyakhovskaya, T M Zimkina, V A Fomichev *Fiz. Tverd. Tela* **12** 138 (1970)
99. V V Odintsov, Yu B Paderno, Yu M Goryachev *Zh. Strukt. Khim.* **2** 344 (1971)
100. A L Ivanovskii, D L Novikov, V I Anisimov *Zh. Strukt. Khim.* **30** 32 (1989)
101. A Neckel *Int. J. Quantum Chem.* **23** 1317 (1983)
102. V P Zhukov, N I Medvedeva, V A Gubanov *Phys. Status Solidi B* **151** 407 (1989)
103. A L Ivanovskii, V P Zhukov, V A Gubanov *Elektronnoe Stroenie Tugoplavkikh Karbidov i Nitridov Perekhodnykh Metallov* (Electronic Structures of Refractory Carbides and Nitrides of Transition Metals) (Moscow: Nauka, 1990)
104. A L Ivanovsky, G P Shveikin *Phys. Status Solidi B* **181** 251 (1994)
105. V I Anisimov, V P Antropov, V A Gubanov, A L Ivanovskii, A I Likhttenshtein, E Z Kurmaev *Elektronnaya Struktura Defektov i Primesei v Metallakh, Splavakh i Soedineniyakh* (The Electronic Structure of Defects and Admixtures in Metals, Alloys and Compounds) (Moscow: Nauka, 1989)
106. P Mohn *J. Phys. C, Solid State* **21** 2841 (1988)
107. D R Armstrong, P G Perkins *Theor. Chim. Acta* **64** 41 (1983)
108. P Mohn, D G Pettifor *J. Phys. C, Solid State Phys.* **21** 2829 (1988)
109. R F Sabiryanov, V L Ivanovskii *Metallofizika* **14** 7 (1992)
110. D R Armstrong, P G Perkins *J. Chem. Soc., Faraday Trans. 2* 12 (1979)
111. T N Bell, P G Perkins *J. Phys. Chem.* **81** 2102 (1977)
112. A R Williams, J Kubler, C D Gelatt *Phys. Rev. B, Solid State* **19** 6094 (1979)
113. M C Cadeville, A J P Meyer *C. R. Acad. Sci.* **255** 3391 (1962)
114. N S Miryasov, A P Parsanov *Izv. Akad. Nauk SSSR, Ser. Fiz.* **23** 285 (1959)
115. N Lundquist, H P Myers *Ark. Fys.* **20** 30 (1961)
116. R Hocart, M Fallot *C. R. Hebd. Seances Acad. Sci.* **203** 1062 (1936)
117. R F Sabiryanov, O N Mryasov, A L Ivanovskii, G P Shveikin *Metallofizika* **13** 71 (1991)
118. A L Ivanovskii, V I Anisimov, V A Gubanov, E Z Kurmaev *Zh. Strukt. Khim.* **27** 3 (1986)
119. A L Ivanovsky *Phys. Status Solidi B* **157** 129 (1990)
120. G V Samsonov, Yu M Goryachev, B A Kovenskaya, E Ya Tel'nik *Izv. Vyssh. Uchebn. Zaved. Fiz.* **6** 37 (1972)
121. J K Burdett, E Canadell, G J Miller *J. Am. Chem. Soc.* **108** 6561 (1986)
122. V M Anishchik, N N Dorozhkin *Phys. Status Solidi B* **160** 173 (1990)
123. G Will, A Kirfel, in *Proceedings of the International Conference on Boron-rich Solids, Albuquerque, New York, 1986* p. 88
124. R O Zaitsev *Sverkhprov. Fiz. Khim. Tekh.* **2** 36 (1989)
125. J Hubbard *Proc. R. Soc. London, Ser. A* **281** 401 (1964)
126. V Emery *Phys. Rev. Lett.* **58** 2797 (1987)
127. F Vahldiek *New Technol. Week* **9** 6 (1989)
128. B Ahern *Supercond. Week* **23** 9 (1989)
129. P J Brown, J L Cox *Philos. Mag.* **23** 705 (1971)
130. R S Perkins, P J Brown *J. Phys. F, Met. Phys.* **4** 906 (1974)
131. D J Joyner, O Johnson, D M Hercules, D W Bullett, J H Weaver *Phys. Rev. B, Solid State* **24** 3122 (1981)
132. R H Multu, A Aidimuraz *J. Magn. Magn. Matter* **68** 328 (1987)
133. I Bakonyi *J. Magn. Magn. Matter* **73** 171 (1988)
134. E J O Garba, R L Jacobs *J. Phys. Chem. Solids* **50** 101 (1989)
135. N E Solov'ev, V S Makarov, Ya A Ugai, in *Boridy i Materialy na Ikh Osnove* (Borides and Materials Based upon Them) (Kiev: Inst. Poroshk. Metallurg. Akad. Nauk Ukr. SSR, 1986) p. 36
136. E I Zornberg *Phys. Rev. B, Solid State* **2** 224 (1970)
137. D G Dempsey, W R Grise, L Kleinman *Phys. Rev. B, Solid State* **17** 1209 (1978)
138. I I Kostetskii, S N L'vov *Fiz. Met. Metalloved.* **34** 475 (1972)
139. I I Kostetskii, S N L'vov *Fiz. Met. Metalloved.* **33** 773 (1972)
140. H Ichara, M Nirabayashi, H Nakagava *Phys. Rev. B, Solid State* **16** 726 (1977)
141. D L Johnson, B N Harman, S H Liu *J. Chem. Phys.* **73** 1989 (1980)
142. L F Mattheiss *Phys. Rev.* **33** 1399 (1964)
143. K Schwarz *Phys. Rev.* **8** 2466 (1957)
144. F S Ham, B Segal *Phys. Rev.* **124** 1786 (1961)
145. B Segal *Phys. Rev.* **105** 108 (1957)
146. G S Painter, D E Ellis *Phys. Rev. B, Solid State* **1** 4747 (1970)
147. T Inoshita, K Nakoo, H Kamimura *J. Phys. Soc. Jpn.* **43** 1237 (1977)
148. N A Holzwarth, S Rabii, L A Girifalco *Phys. Rev. B, Solid State* **18** 5190 (1978)
149. R C Linton *Thin Solid Films* **20** 17 (1974)
150. J M Ziman *Principles of the Theory of Solids* (New York: Cambridge University Press, 1972)
151. A L Ivanovskii, Thesis in Chemical Sciences, Institute of Chemistry, Urals Div. Acad. Sci. USSR, Sverdlovsk, 1988

152. D R Armstrong *J. Less-Common Met.* **67** 191 (1979)
153. S La Placa, B Post *Acta Crystallogr.* **15** 97 (1962)
154. W Trzebiatowski, J Rudzinski *J. Less-Common Met.* **6** 244 (1964)
155. R Hoffmann *J. Chem. Phys.* **39** 1397 (1963)
156. D L Novikov, A L Ivanovskii, V A Gubanov *Zh. Neorg. Khim.* **33** 2673 (1988)
157. A N Pilyankevitsh, V K Rasovenov, G L Zhounkovsky, in *VI Int. Pulvermetal. Tagung B. 2, Dresden, 1977* p. 441
158. S S Ordan'yan, V I Unrod, A K Avgustinnik *Poroshk. Metall.* **9** 40 (1975)
159. J D Venables *Philos. Mag.* **16** 873 (1967)
160. G L Zhunkovskii, T M Evtushok, S A Shvab, in *Boridy i Materialy na Ikh Osnove* (Borides and Materials Based upon Them) (Kiev: Inst. Poroshk. Metallurg. Akad. Nauk Ukr. SSR, 1986) p. 91
161. O F Chernysheva, V S Sinel'nikov, T Ya Kosolapova *Izv. Akad. Nauk SSSR, Neorg. Mater.* **15** 614 (1979)
162. G V Samsonov, in *Voprosy Poroshkovoi Metallurgii i Prochnosti Materialov* (Problems in Powder Metallurgy and the Strength of Materials) No VII (Kiev: Izd. Akad. Nauk Ukr. SSR, 1959) p. 72
163. G G Smirnov, Author's Abstract of Candidate Thesis in Technical Sciences, Leningrad Technol. Inst., Leningrad, 1971
164. A L Borisova *Sovmestimost' Tugoplavkikh Soedinenii s Metallami i Grafitom* (Compatibility of Refractory Compounds with Metals and Graphite) (Kiev: Nauk. Dumka, 1985)
165. R Kiffer, F Benzenovskii *Tverdye Materialy* (Solid Materials) (Moscow: Metallurgiya, 1968)
166. V V Pakholkov, I V Brettser-Portnov, I G Grigorov, Yu G Zainulin *Izv. Akad. Nauk SSSR, Neorg. Mater.* **16** 873 (1993)
167. V I Anisimov, A L Ivanovskii, V A Gubanov, E Z Kurmaev *Zh. Strukt. Khim.* **27** 3 (1986)
168. A L Ivanovsky, V I Anisimov, A I Lichtenstein, V A Gubanov *J. Phys. Chem. Solids* **49** 479 (1988)
169. R F Sabiryanov, Author's Abstract of Candidate Thesis in Physicomathematical Sciences, Inst. Chem. Solids, Urals Div. Russ. Acad. Sci., Ekaterinburg, 1993
170. J F Halet, J Y Saillard, J Bauer *J. Less-Common Met.* **158** 239 (1990)
171. J Bauer, M Potel, J Geogeon, in *Proceedings of the IXth International Conference on Solid Compounds of Transition Elements, Dalton Division, Oxford, 1988* p. 112
172. J Bauer, O Bars *Acta Crystallogr., Sect. B* **36** 1540 (1980)
173. W N Lipscomb *J. Less-Common Met.* **82** 1 (1981)
174. W Hume-Rothery, G V Raynor *The Structure of Metals and Alloys* (Translated into Russian; Moscow: Metallurgiya, 1959)
175. I I Kornilov *Izv. Akad. Nauk SSSR, Metall. Gorn. Delo* **6** 19 (1964)
176. I I Kornilov *Metally i Vzaimodeistviya mezhdu Nimi* (Metals and Interactions between Them) (Moscow: Nauka, 1964)
177. E S Makarov *Dokl. Akad. Nauk SSSR* **186** 313 (1969)
178. I I Kornilov *Dokl. Akad. Nauk SSSR* **81** 597 (1951)
179. I I Kornilov, N M Matveeva, L I Pryakhina, R S Polyakova *Metallokhimicheskie Svoistva Elementov Periodicheskoi Sistemy* (Metallochemical Properties of the Elements) (Moscow: Nauka, 1966)
180. V N Troitskii, B N Grebtsov, M I Aivazov *Poroshk. Metall.* **3** 6 (1973)
181. Ya A Krestin'sh, U A Tsielen, V Ya Bondars, in *Dispersionnye Kristallicheskie Poroshki v Materialovedenii* (Dispersed Crystalline Powders in Materials Technology) (Kiev: Inst. Poroshk. Metallurg. Akad. Nauk Ukr. SSR, 1980) p. 16
182. T Ya Kosolapova, E M Dudnik, O P Kulik, in *Boridy i Materialy na Ikh Osnove* (Borides and Materials Based upon Them) (Kiev: Inst. Poroshk. Metallurg. Akad. Nauk Ukr. SSR, 1986) p. 13
183. J Y Cautarel, H Pastor, R Meyer, in *Plansee Seminar, Reutte Austria, 1974* p. 12
184. H Nowotny, F Benesovsky, C Brukl, O Schob *Monatsh. Chem.* **92** 403 (1961)
185. Yu G Zainulin, S I Alyamovskii, G P Shveikin *Izv. Akad. Nauk SSSR, Neorg. Mater.* **12** 1581 (1976)
186. A L Ivanovskii, Yu G Zainulin, V A Gubanov *Zh. Neorg. Khim.* **30** 579 (1985)
187. A L Ivanovsky, V A Gubanov, G P Shveikin, V I Anisimov *J. Phys. Chem. Solids* **47** 275 (1986)
188. A Lebugle, R Nyholm, N Martensson *J. Less-Common Met.* **82** 265 (1981)
189. V P Zhukov, N I Medvedeva, G P Shveikin *Izv. Akad. Nauk SSSR, Neorg. Mater.* **28** 1402 (1992)
190. Ya V Buran, Ya O Dovgii, I V Kityk *Fiz. Tverd. Tela* **31** 275 (1989)
191. G Will, A Kirfel, B Josten *J. Less-Common Met.* **82** 255 (1981)
192. M Krogh *Acta Crystallogr., Sect. B* **24** 179 (1968)
193. Ya V Burak, Ya O Dovgii, I V Kityk *Zh. Prikl. Spektrosk.* **51** 745 (1989)
194. W Harrison *Electronic Structure and the Properties of Solids* Vol. 2 (Translated into Russian; Moscow: Mir, 1983)
195. A Kirfel, A Gupta, G Will *Acta Crystallogr., Sect. B* **38** 1311 (1980)
196. A Kirfel, A Gupta, G Will *Acta Crystallogr., Sect. B* **35** 1052 (1979)
197. A Kirfel, A Gupta, G Will *Acta Crystallogr., Sect. B* **35** 2291 (1979)
198. W H Zacharasen *Acta Crystallogr., Sect. B* **17** 749 (1964)
199. A Amamon *Phys. Status Solidi A* **54** 565 (1979)
200. L Tokacs *Solid State Commun.* **21** 611 (1977)
201. A C Switendick *Solid State Commun.* **19** 511 (1976)
202. A Amamon, G Krill *Solid State Commun.* **33** 1087 (1980)
203. P H Citrin, G K Wertheim, Y Boer *Phys. Rev. Lett.* **41** 1425 (1978)
204. G K Wertheim, G Crecelius *Phys. Rev. Lett.* **40** 813 (1978)
205. Zong-Quan Gu, W Y Ching *J. Magn. Magn. Mater.* **54/57** 525 (1986)
206. J Inoue, M Shimizu *J. Phys. F, Met. Phys.* **16** 1051 (1986)
207. J Inoue, M Shimizu *J. Phys. F, Met. Phys.* **16** 1157 (1986)
208. M Sagawa, S Fujiwara, N Tagawa, H Yamamoto, Y Matsuura *J. Appl. Phys.* **55** 2083 (1984)
209. H Yamaguchi, M Yamada, Y Yamaguchi, H Yamamoto, S Hirosawa, M Sagawa *J. Magn. Magn. Mater.* **54/57** 413 (1986)
210. K Handrik, S Kobe *Amorphous Ferro- and Ferrimagnetic Substances* (Translated into Russian; Moscow: Mir, 1982)
211. D S Boudreaux *Phys. Rev. B, Solid State* **18** 4039 (1978)
212. C R Nagel, J Tauc *Phys. Rev. Lett.* **35** 380 (1975)
213. D E Polk *Acta Metall.* **20** 485 (1972)
214. H S Shen, B P Park *Acta Metall.* **21** 395 (1973)
215. R P Messmer *Phys. Rev. B, Solid State* **23** 1616 (1981)
216. V V Nemoshkalenko, A P Shpak, I P Nagibin, A N Yares'ko V L Karbovskii *Metallofizika* **4** 82 (1990)
217. J Wong, F W Lytle, R B Greegor, in *Rapidly Quenched Metals III* Vol. 2 (Ed. B Cantor) (London: Metal Society, 1978) p. 345
218. A V Postnikov, Candidate Thesis in Physicomathematical Sciences, Inst. Phys. Math. Urals Div. Acad. Sci. USSR, Sverdlovsk, 1985
219. P Lamparter, E Nodl, G Rainer *Hartbach. Ztschr. Naturforsch.* **A36** 165 (1981)
220. N Cowlan, G E Carr *J. Phys. F, Met. Phys.* **15** 1117 (1985)
221. D S Boudereaux, H J Frost *Phys. Rev. B, Solid State* **23** 1506 (1981)
222. M Krajci, P Mrafko *J. Phys. F, Met. Phys.* **18** 2137 (1988)
223. I Turek, J Yafner, Ch Hausleitner *J. Magn. Magn. Mater.* **109** L145 (1992)
224. Y Kakehashi *Phys. Rev. B, Solid State* **43** 10 820 (1991)
225. D N Manh, G D Hoai, A Pasturel, C Colinet *Physica B* **173** 293 (1991)
226. H J Nowak, O K Andersen, T Fujiwara, O Jepsen *Phys. Rev. B, Solid State* **44** 3577 (1991)
227. I Turek *J. Phys., Condens. Matter* **2** 10 559 (1990)
228. T Fujiwara *J. Phys. F, Met. Phys.* **12** 661 (1982)
229. T Fujiwara, H S Chen, Y Wasada *J. Phys. F, Met. Phys.* **11** 1327 (1981)
230. I Turek *J. Magn. Magn. Mater.* **98** 119 (1991)
231. H Tanaka, S Takayama, M Hasegawa *Phys. Rev. B, Solid State* **47** 2671 (1993)
232. V V Nemoshkalenko, A P Shpak, V L Karbovskii *Metallofizika* **12** 24; 129 (1990)
233. E Majkova, P Duhaj *Phys. Status Solidi B* **146** K17 (1988)
234. T I Bratus', M A Vasil'ev, V T Cherepin *Metallofizika* **5** 71 (1983); **6** 77 (1984)
235. P Marko, O Dusha, L Pototski *Poverkhn. Fiz. Khim. Mekhan.* **3** 68 (1984)
236. P P Karve, S K Kulkarnai, A S Nigavekar *Solid State Commun.* **49** 719 (1984)
237. P Sen, A Srinivasan, M S Hedge, C N O Rao *J. Mater. Sci.* **18** 173 (1983)
238. D R Baer, M T Thomas *J. Vac. Sci. Technol.* **18** 722 (1981)
239. M Matsuura, T Namoto, F Itoh, K Suzuki *Solid State Commun.* **33** 895 (1980)

240. D R Baer, D A Petersen, L R Pederson, M T Thomas *J. Vac. Sci. Technol.* **20** 957 (1982)
241. P P Karve, M G Thube, S K Kulkarnai, A S Nigavekar *Solid State Commun.* **50** 1027 (1984)
242. V V Nemoshkalenko, D E Ovsienko, D Yu Paderno, in *"Issledovanie Struktury Amorfnykh Metallicheskikh Splavov". Tezisy Dokladov Vsesoyuznoi Konferentsii, Moskva, 1990* (Abstracts of Reports at the All-Union Conference "Investigation of the Structures of Amorphous Metal Alloys", Moscow, 1990) p. 119
243. S Kapusta, K E Heusler *Z. Metallkd.* **72** 785 (1981)
244. B V Molotilov, A I Zakharov, A G Narmonev, in *"Rentgenovskie i Rentgenoelektronnye Spektry i Elektronnaya Struktura Splavov i Soedinenii". Tezisy Dokladov Vsesoyuznoi Konferentsii, Izhevsk, 1979* (Abstracts of Reports at the All-Union Conference "X-Ray and X-Ray Electron Spectra and the Electronic Structures of Alloys and Compounds", Izhevsk, 1979) p. 105
245. B V Molotilov, A I Zakharov, A G Narmonev *Fiz. Met. Metalloved.* **51** 1106 (1981)
246. N Lustig, L J Pilione, K C Woo, J S Lannin *J. Non-Cryst. Solids* **61/62** 1295 (1984)
247. S Ray, J Tauc *Solid State Commun.* **34** 769 (1980)
248. S Falch, G Rainer-Harbach, F Schmueckle, S Steeb *Z. Naturforsch. A, Phys. Sci.* **36** 937 (1981)
249. A Amamon, G Krill *Solid State Commun.* **31** 971 (1979); **33** 1087 (1980)
250. V V Nemoshkalenko, A I Senkevich, S I Latynov, A G Dmitriev *Metallofizika* **7** 18 (1985)
251. J L Walter, F Bacon, F E Liborsky *Mater. Sci. Eng.* **24** 239 (1976)
252. E Cartier, Y Baer, M Liard, H-J Guentherodt *J. Phys. F, Met. Phys.* **10** L21 (1980)
253. K Tanaka, M Yoshino, K Suzuki *J. Phys. Soc. Jpn.* **51** 3882 (1982)
254. A J Bevolo, C S Severin, C W Chen *J. Vac. Sci. Technol.* **20** 852 (1982)
255. K Hricovind, J Krempasky *J. Phys. F, Met. Phys.* **15** 1321 (1985)